

Review

# N-Annulated Perylene Diimide Non-Fullerene Acceptors for Organic Photovoltaics

Mahmoud E. Farahat <sup>\*,†</sup>  and Gregory C. Welch <sup>\*</sup> 

Department of Chemistry, University of Calgary, 2500 University Drive N.W., Calgary, AB T2N 1N4, Canada

\* Correspondence: mahmoud.farahat@ucalgary.ca or mahmoud.farahat@nrc-cnrc.gc.ca (M.E.F.); gregory.welch@ucalgary.ca (G.C.W.)

† Current Address: Advanced Electronics and Photonics Research Centre, National Research Council Canada, 1200 Montreal Road, Ottawa, ON K1A 0R6, Canada.

**Abstract:** This work covers the development of non-fullerene acceptors for use in organic photovoltaics built using the N-annulated perylene diimide dye. The classic perylene diimide dye has been extensively used to construct non-fullerene acceptors, leading to device power conversion efficiencies of over 10%. Strong visible light absorption and deep frontier molecular energy levels have made such materials (both molecular and polymeric) near ideal for pairing with narrow-gap conjugated polymers in bulk-heterojunction active layers. The N-annulation of the dye provides an extra site for side-chain engineering and alters the electronic structure of the polycyclic aromatic core. In addition, N-annulation allows for selective bromination of the perylene core, leading to building blocks that are useful for the construction of large molecular frameworks using the atom-economical direct heteroarylation cross-coupling method. Herein, we detail a series of molecules developed by our team that are based on the N-annulated perylene diimide in the form of dimers with different cores (both electron-rich and electron-deficient); dimers with varied side chains; tetramers with varying geometries; and large, asymmetric molecules with internal energy cascades. The use of these molecules as non-fullerene acceptors in organic photovoltaic devices (binary and ternary blends, outdoor and indoor light applications, and spin-coated vs. slot-die-coated photoactive layers) is presented.

**Keywords:** photovoltaic devices; Organic Solar Cells; non-fullerene acceptors; perylene diimide dyes



**Citation:** Farahat, M.E.; Welch, G.C. N-Annulated Perylene Diimide Non-Fullerene Acceptors for Organic Photovoltaics. *Colorants* **2023**, *2*, 151–178. <https://doi.org/10.3390/colorants2010011>

Academic Editors: Nadia Barbero, Carlotta Pontremoli and Simone Galliano

Received: 10 February 2023

Revised: 9 March 2023

Accepted: 16 March 2023

Published: 21 March 2023



**Copyright:** © 2023 by the authors. Licensee MDPI, Basel, Switzerland. This article is an open access article distributed under the terms and conditions of the Creative Commons Attribution (CC BY) license (<https://creativecommons.org/licenses/by/4.0/>).

## 1. Introduction

Organic photovoltaics (OPVs) have features that include being lightweight [1], flexible, and stretchable [2], compatible with additive manufacturing [3,4], and color-tunable for windows and building integration applications [5–8]. They are thus considered a potentially game-changing clean energy technology. Figure 1 summarizes selected applications to highlight the versatility and promising future of OPVs. Jinno et al. developed stretchable and washable textile-compatible OPVs (Figure 1a), paving the way towards wearable devices [9]. The industrial sector and startups have contributed heavily to OPV development, with InfinityPV having created both flexible OPV modules and tapes (Figure 1b,c), Next Energy Technologies, Inc. having introduced transparent OPVs for building windows (Figure 1d), ARMOR having developed large-area flexible and semi-transparent OPV films that serve a wide range of applications (Figure 1e), and Heliatek having commercialized vacuum-deposited films for building-integrated OPVs (BIOPVs) (Figure 1f,g), while both Dracula Technologies and Epishine are developing OPV mini-modules for indoor light harvesting (Figure 1h,i).

The first OPV devices, reported by Tang in 1986, made use of a bilayer heterojunction architecture composed of two thermally evaporated films (phthalocyanine as the donor and a perylene derivative as the acceptor). They had a power conversion efficiency (PCE) of 1% [10,11]. A decade later (1995), Prof. Alan Heeger and coworkers introduced solution-processed bulk heterojunction (BHJ) OPV devices based on fullerene acceptors [12]. The

BHJ active layers are typically composed of interpenetrating networks of a donor (polymer and/or small molecule) [13–15] and an acceptor (typically a fullerene derivative) [16–18] sandwiched between two charge-transport layers with conductive electrodes on each side [19,20]. The nanomorphology and phase separation between the donor and acceptor in these BHJ films is critical to performance and as such has been well studied [21–23]. A typical OPV device architecture is illustrated in Figure 1j.

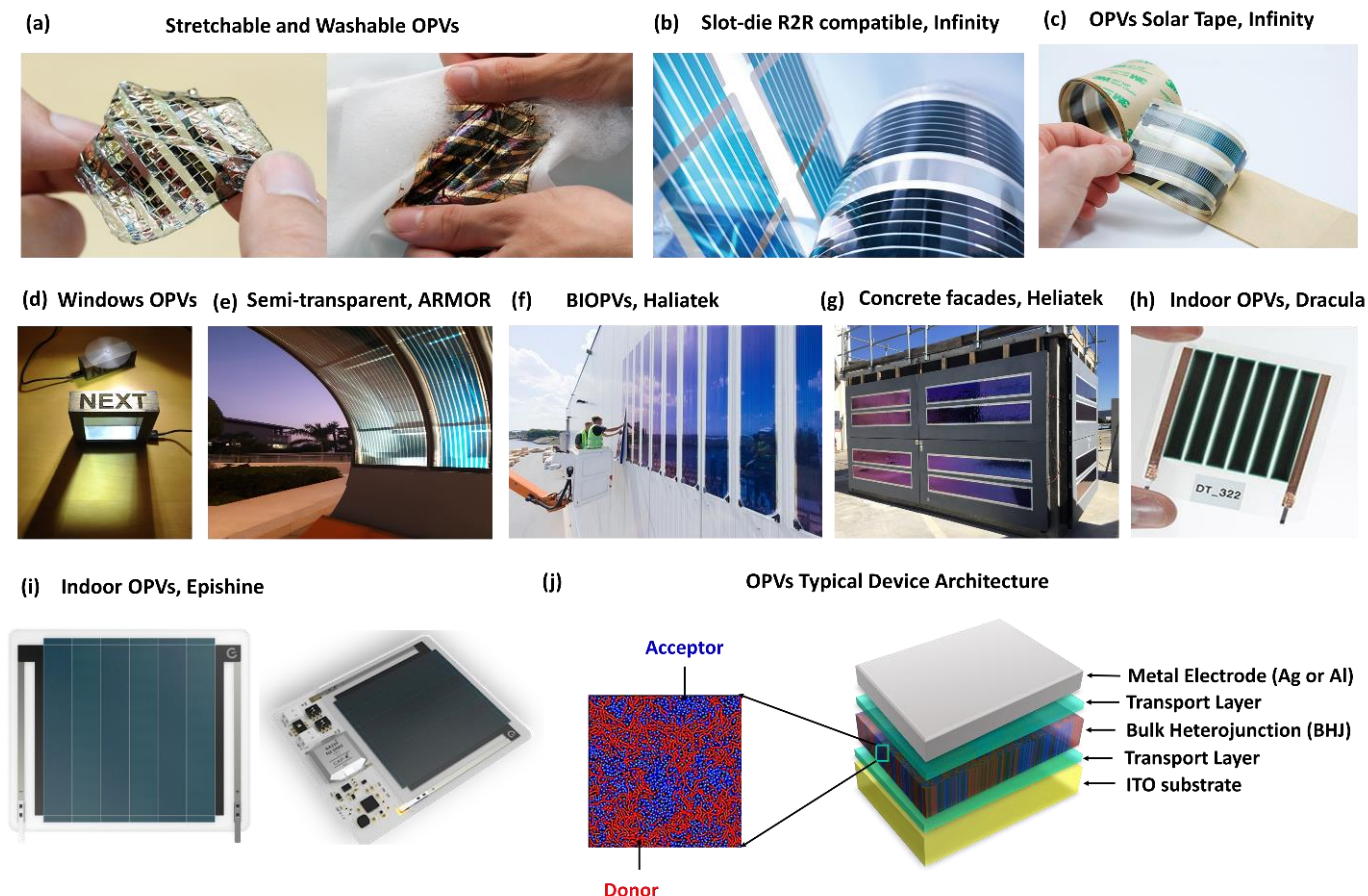


**Figure 1.** Examples showing versatile applications of OPVs: (a) stretchable and washable OPV devices for wearable applications [9], (b) slot-die-coated flexible OPV modules from InfinityPV, (c) OPV solar tape from InfinityPV, (d) transparent OPV windows by Next Energy Technologies, Inc., (e) semi-transparent OPVs by ARMOR, (f,g) building-integrated OPVs (BIOPVs) by Haliatek, (h) indoor OPV mini module by Dracula, (i) mini modules for integrated indoor IoT sensors by Epishine, and (j) schematic illustration of a typical OPV device architecture (active layer morphology is shown as zoomed-in image) [24]. Images in (a,j) reproduced with permission from [9,24]. Copyright 2017, Springer Nature and 2011, Royal Society of Chemistry. All images are used with permission.

For two decades, OPVs were primarily based upon fullerene acceptors (PC<sub>61</sub>BM [25], PC<sub>71</sub>BM [26], Figure 2). Such fullerenes demonstrate good solubility in organic solvents, have a high electron affinity and electron mobility, and are thermally stable. Paired with molecular or polymeric donors, fullerenes form suitable nanomorphologies with appropriate phase separation, leading to BHJ active layers with efficient charge generation and balanced charge transport [18,27]. OPVs based upon these fullerene acceptors (e.g., PC<sub>61</sub>BM, PC<sub>71</sub>BM, and ICBA) have a PCE of approximately 12% [28–30]. In parallel, there has always been interest in the development of non-fullerene acceptors (NFAs), with recent successes resulting in PCEs increasing from low values of 0.5% for devices based on perylene diimide molecules (PDI-3) in 2010 to 18% for devices based on ring-fused

donor–acceptor molecules [31–35]. Recently, Firdaus et al. predicted the realization of 20% PCEs for single-junction OPVs based upon the use of NFAs [36].

The primary parameters for the development of OPVs include: efficiency, lifetime, and production cost (e.g., upscaling) [37]. A module efficiency > 10% with operational stability > 10 years combined with a production cost << EUR 1 per Watt peak is suggested for the industrial production of OPVs [37,38]. The cost of semitransparent OPVs (with PCEs > 10%) processed via a roll-to-roll (R2R) manufacturing line is expected to be USD 1.6 per Watt peak [39]. With PCEs reaching over 19% at the lab scale, the transition from lab to fab is becoming a priority [40]. A recent study demonstrated an OPV mini-module (active area of 32.6 cm<sup>2</sup>) processed from eco-friendly solvents under ambient condition with a PCE of 10.3% under 1 sun illumination [41]. Similarly, flexible OPV mini-modules have been R2R coated in air, delivering a PCE of 13.4% under indoor office light conditions [42].

Since OPVs retain high performance under indoor illumination conditions, the technology is an ideal candidate for powering smart devices for the internet of things (IoT) [43]. Such smart devices only require low power inputs and can be operated using the electricity generated from OPV devices in low-intensity light environments [44–48], thus presenting a new application for OPVs. In addition to OPVs being a viable clean energy technology for low-light-intensity applications, large-area installations, building and transportation integration, and greenhouses, the field of OPVs offers a rich training platform for young scientists to learn and discover the fundamentals of organic materials design and synthesis, electron transfer processes, supramolecular chemistry, photochemistry, interface science, and ink formulations and printing. As such, the field has been subject to numerous review articles [15,49–53].

## 2. Non-Fullerene Acceptors

There has been a large variety of NFAs reported that have been designed with specific physical characteristics, optoelectronic properties, and self-assembly tendencies [54,55]. They can have wide or narrow optical band gaps, shallow or deep frontier molecular orbital (FMO) energy levels, be rendered solution-processible from green solvents and, most importantly, be tailored for pairing with a specific molecular or polymeric donor material. The breakthrough in the design of NFAs began with the introduction of ITIC [56] and its optimized version, IT-4F [57] (Figure 2). PBDB-T:IT-4F blends achieved an OPV device PCE of 13% and were therefore some of the first reports of NFA-based OPVs outperforming fullerene-based OPVs. A strongly NIR-absorbing NFA (Y series) was introduced in early 2019 and has led to NFA-based OPVs with PCEs beyond 19% [58] (Figure 2).

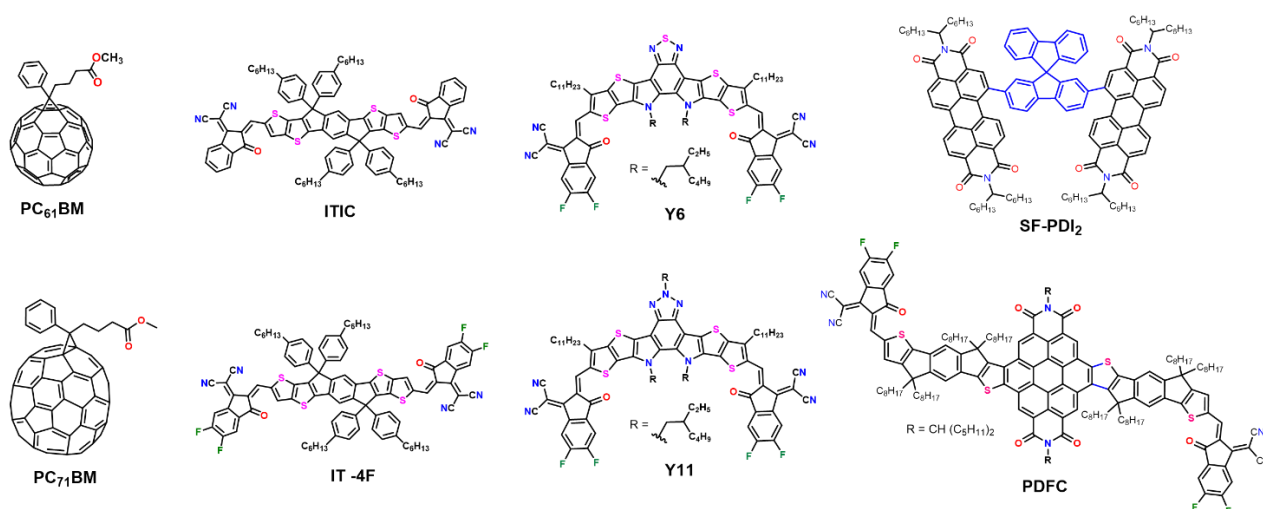


**Figure 2.** Chemical structures of PC<sub>61</sub>BM [25], PC<sub>71</sub>BM [26], ITIC [56], IT-4F [57], Y6 [59], Y11 [60], SF-PDI<sub>2</sub> [61], and PDFC [62] as representative acceptors for high-performance OPV devices.

Among the best NFAs are those built upon the perylene diimide (PDI) chromophore. Facile functionalization at the imide, bay, and headland positions allows for structural engineering to tailor solubility parameters, optoelectronic properties, and self-assembly tendencies. As such, hundreds of PDI-based molecules have been constructed and utilized as NFAs, and the field has been reviewed in depth [63–70]. Devices with binary BHJs with a PCE of 9.5% (open-circuit voltage ( $V_{oc}$ ) = 1.11 V; short-circuit current ( $J_{sc}$ ) = 13.3 mA/cm<sup>2</sup>; fill factor (FF) = 64%) were achieved when using the twisted PDI dimer (SF-PDI<sub>2</sub>) blended with the P3TEA polymer donor [61] (Figure 2). Devices with a PCE of over 10% were achieved by employing the ternary approach using a PDBT-T1:SdiPDI-Se:ITIC blend [71]. The PDI tetramer (FTTB-PDI<sub>4</sub>, Figure 3) emerged as excellent NFA and has enabled high-PCE devices (ca. 27%) under low-light illumination (ca. 1650 lux), pushing forward the field of indoor photovoltaics [72,73]. The chemical structure of the selected PDI examples (monomer [74,75], dimer [76,77], trimer [78], and tetramer [72]) are shown in Figure 3.

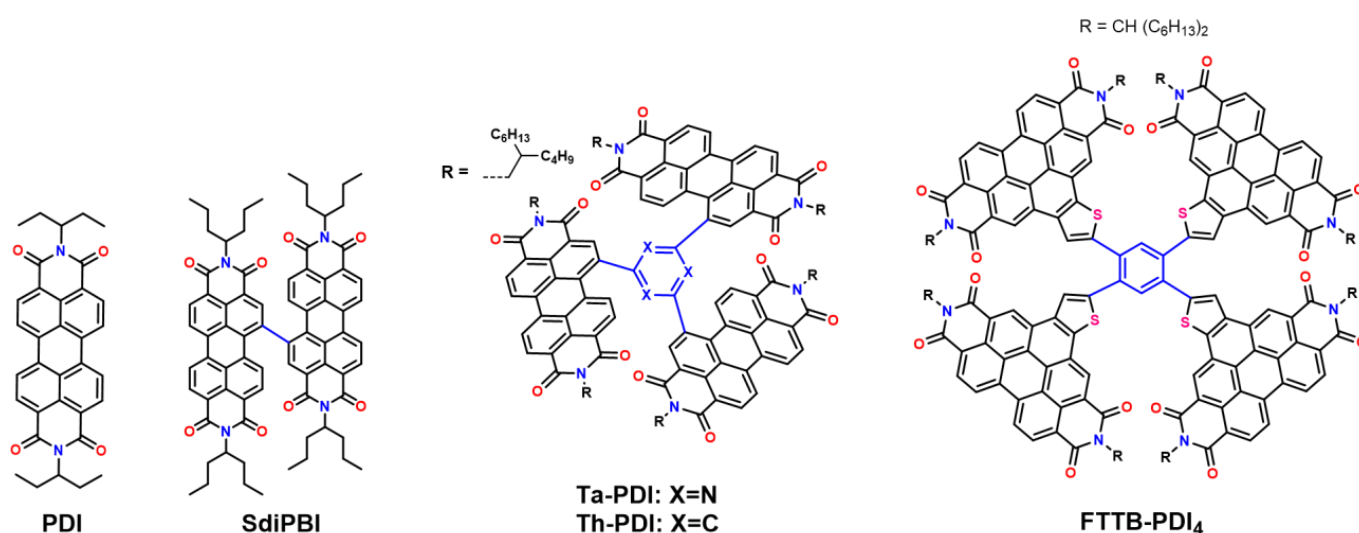


**Figure 3.** Chemical structures of selected example of PDI monomer [74,75], PDI dimer [79], PDI trimer [78], and PDI tetramer [72] NFAs used in OPV devices.

### 3. N-Annulated PDI-Based NFAs

A class of PDI-based NFAs are those based on N-annulated PDI dye. While first reported in 2000 by Langhals et al. [80], our research team, in collaboration with Yan's group, re-introduced the N-annulated PDI as a useful building block for constructing NFAs for OPVs [81]. We first disclosed an OPV device PCE of 7.5% with a high  $V_{oc}$  > 1 V using a N-annulated PDI dimer paired with the P3TEA polymer donor. N-annulation at the bay position of the PDI chromophore allows for installation of functional groups that can fine-tune solubility (e.g., rendering the NFAs soluble in green solvents suitable for large-area processing), self-assembly (e.g., side-chain engineering to increase or decrease the propensity to crystallize), and optical and electronic properties (e.g., the addition of the pyrrole moiety destabilizes the frontier molecular orbital energy levels) [82–84]. With respect to the latter, the N-annulation of PDI raises the LUMO energy level of the PDI by approximately 0.2 eV, and thus various derivatives used as NFAs have led to OPVs with a high operating  $V_{oc}$  that exceeds 1.2 V when paired with wide-gap donor molecules [85]. Another key feature of the N-annulated PDI is that bromination is selective in the opposite bay position, leading to a building block that can be used to construct PDI-core-PDI-type molecular frameworks (vide infra). In this personal account, we provide a complete survey of our group's development of N-annulated PDIs for use as photoactive materials in OPV devices. Beyond OPV device performance, we present efforts towards upscaling and indoor light recycling. The chemical structures and electronic energy levels of the N-annulated PDIs are presented in Figures 4 and 5, respectively. The chemical structures of the donor

materials are shown in Figure 5, and the OPV parameters are summarized in Table 1. All devices were fabricated in air using the inverted device architecture: ITO/ZnO/BHJ active layer/MoO<sub>x</sub>/Ag unless stated otherwise.

### Core-based Dimers

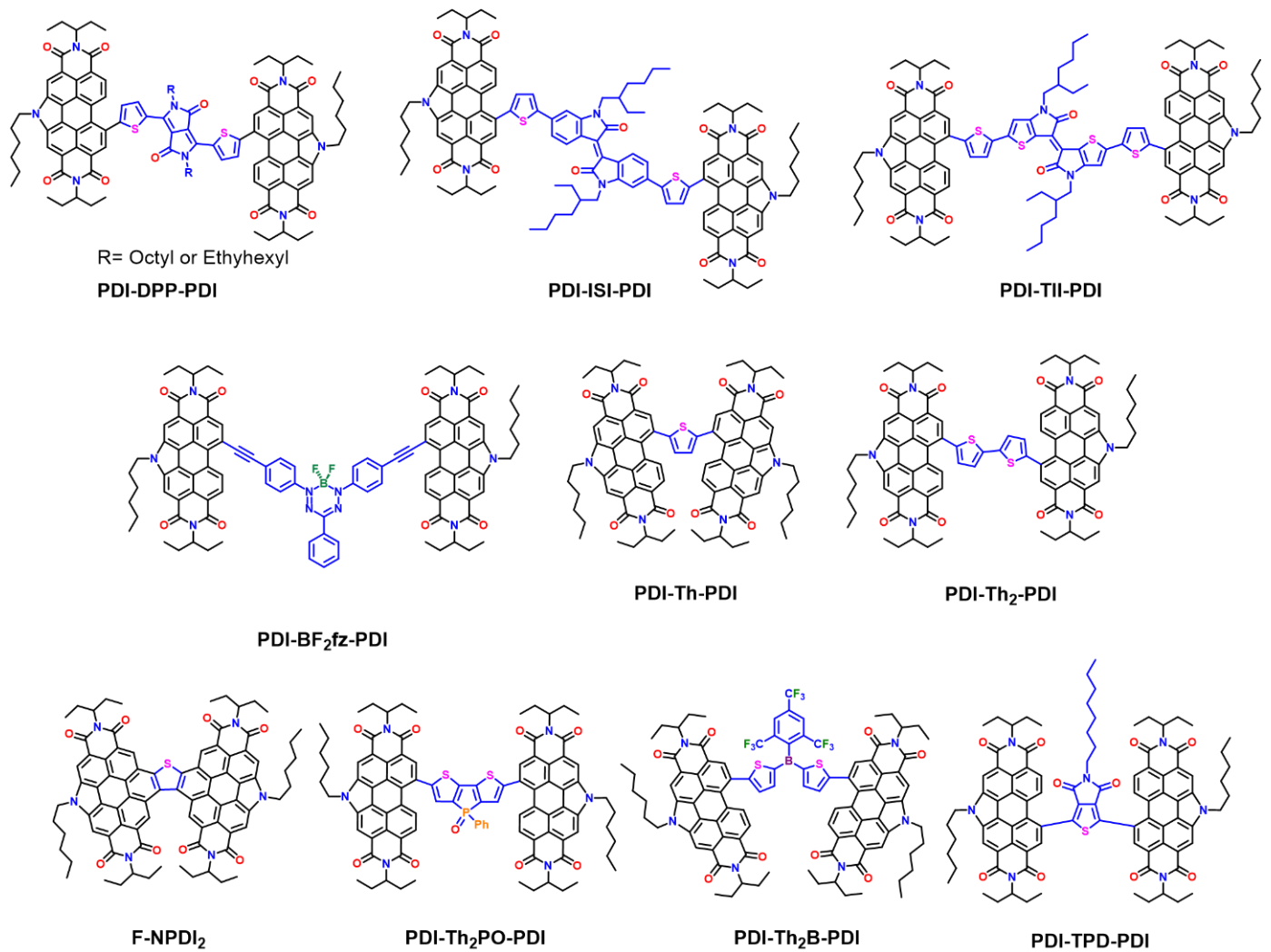
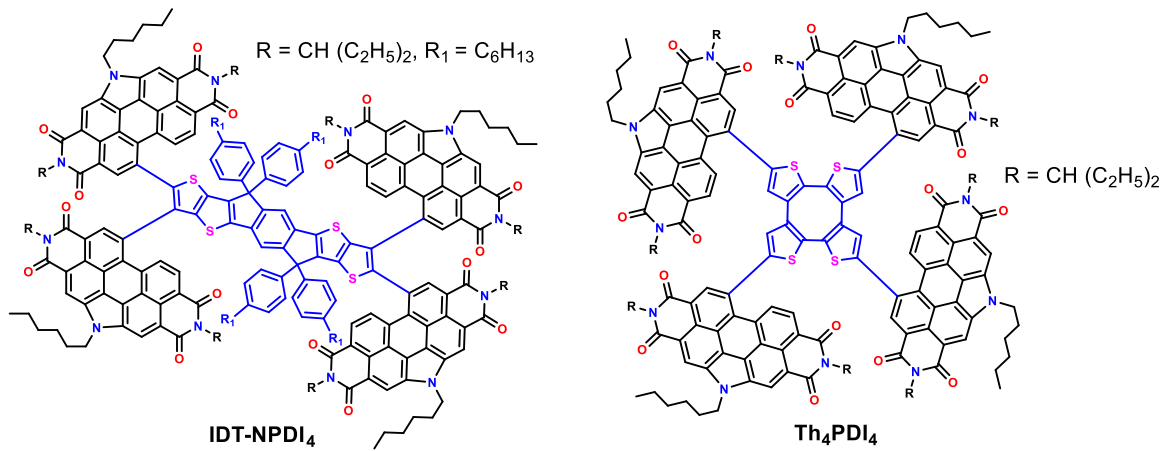
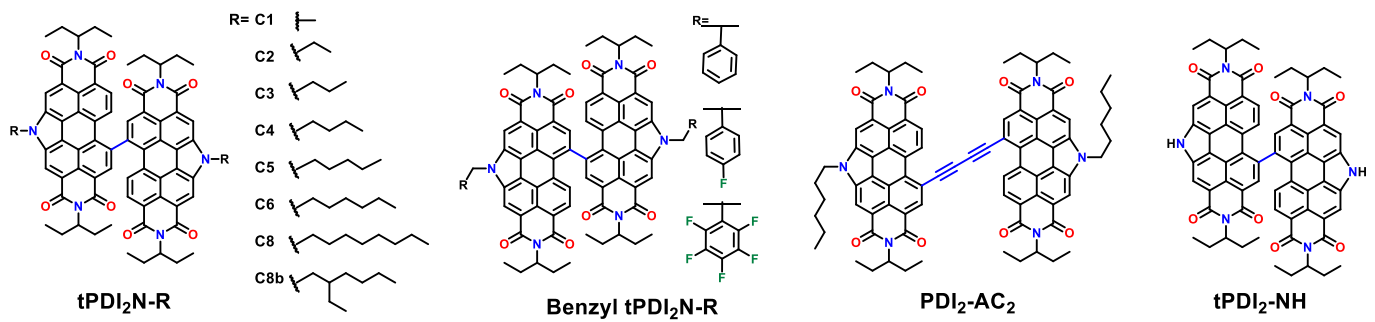


Figure 4. Cont.

### Tetramers



### Varied side-chain and acetylene core dimers



### Asymmetric dimers

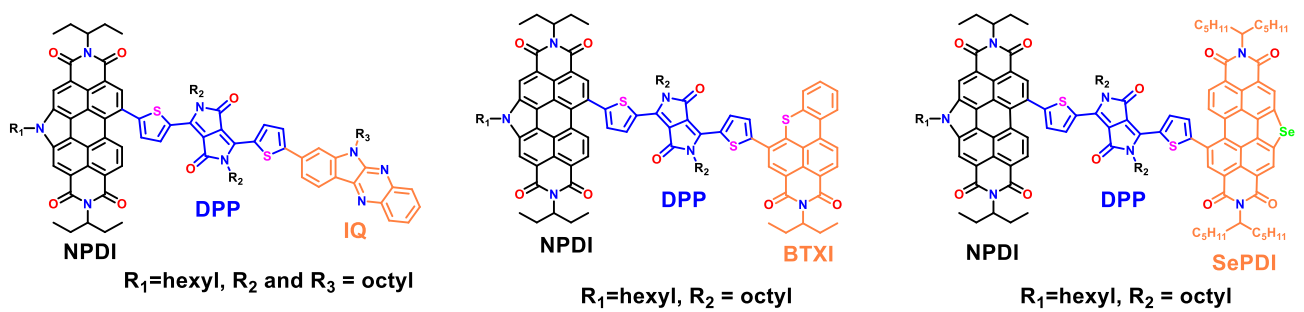


**Figure 4.** Chemical structures of N-annulated PDI-based materials introduced by our research team, used as NFAs in OPV devices and covered in this review.

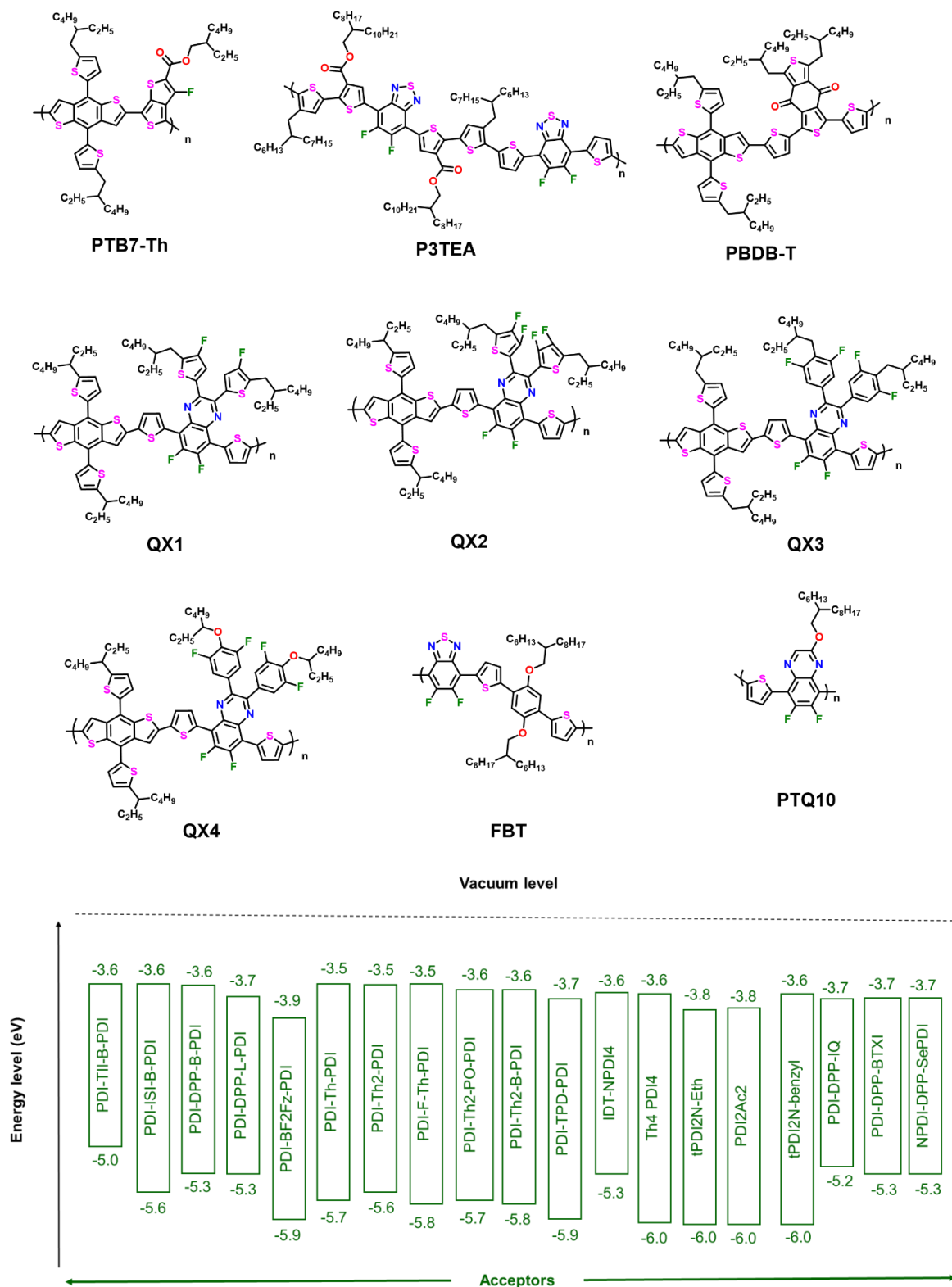


**Figure 5.** (Top) Chemical structures of donor polymers used to pair with N-annulated PDI NFAs in BHJ OPV devices. (Bottom) Electronic energy levels of selected N-annulated PDI NFAs presented in this review. All values determined via cyclic voltammetry (CV).

**Table 1.** Summary of the optoelectronic properties of PDI-Core-PDI dimers, PDI<sub>4</sub> tetramers, PDI<sub>2</sub> dimers, and asymmetric PDIs and the corresponding photovoltaic characteristics based on BHJ OPV devices.

Compound	E <sub>g</sub> (eV)	LUMO (eV)	HOMO (eV)	V <sub>oc</sub> (V)	J <sub>sc</sub> (mA cm <sup>-2</sup> )	FF (%)	PCE (%)	Donor	Processing Cond.	Ref.
PDI-Core-PDI for binary OPVs										
PDI-TII-B-PDI	1.4	−3.6	−5.0	0.93	1.1	34	0.4	PTB7-Th	As-cast	[86]
PDI-ISI-B-PDI	2.0	−3.6	−5.6	1.03	7.0	38	2.6	PTB7-Th	As-cast	[86]
PDI-DPP-B-PDI	1.7	−3.6	−5.3	0.97	6.0	50	2.9	PTB7-Th	0.5% DIO	[86]
PDI-DPP-L-PDI	1.7	−3.7	−5.3	0.98	11.3	50	5.6	PTB7-Th	5 min SVA	[84]
PDI-DPP-L-PDI	1.7	−3.7	−5.3	1.03	10.4	48	5.1	TTFQx-T1	10 min SVA	[87]
PDI-BF <sub>2</sub> fz-PDI	2.0	−3.9	−5.9	0.65	2.0	48	0.6	PPDT2FBT	5 min SVA	[88]
PDI-Th-PDI	2.2	−3.5	−5.7	0.99	5.6	37	2.0	PTB7-Th	As-cast	[89]
PDI-Th <sub>2</sub> -PDI	2.0	−3.5	−5.6	1.05	7.2	36	2.6	PTB7-Th	As-cast	[89]
PDI-F-Th-PDI	2.3	−3.5	−5.8	1.10	7.3	33	2.7	PTB7-Th	1% DMN	[90]
PDI-Th <sub>2</sub> -PO-PDI	2.1	−3.6	−5.7	1.00	5.4	37	2.0	PTB7-Th	0.5% DIO	[91]
PDI-Th <sub>2</sub> -B-PDI	2.2	−3.6	−5.8	1.03	10.0	37	3.9	TTFQx-T1	5% DPE + TA	[92]
PDI-TPD-PDI	2.2	−3.7	−5.9	1.05	7.4	42	3.3	PBDB-T	3% DPE	[93]
(PDI <sub>4</sub> tetramers): PDI <sub>2</sub> -Core-PDI <sub>2</sub> for binary OPVs										
IDT-NPDI <sub>4</sub>	1.7	−3.6	−5.3	1.02	9.6	35	3.4	PTB7-Th	3% CN	[94]
Th <sub>4</sub> PDI <sub>4</sub>	2.1	−3.6	−5.7	0.99	10.6	43	4.5	PTB7-Th	3% CN	[95]
PDI <sub>2</sub> dimer for binary OPVs										
tPDI <sub>2</sub> N-Hex	2.2	−3.8	−6.0	0.89	11.8	49	5.1	PTB7-Th	As-cast	[81]
tPDI <sub>2</sub> N-Et	2.2	−3.8	−6.0	1.13	11.0	61	7.6	P3TEA	2.5% ODT	[81]
tPDI <sub>2</sub> N-Hex	2.2	−3.8	−6.0	1.03	12.5	49	6.3	TTFQx-T1	TA @180 °C	[96]
PDI <sub>2</sub> Ac <sub>2</sub>	2.2	−3.8	−6.0	0.95	4.4	32	1.3	PTB7-Th	As-cast	[97]
tPDI <sub>2</sub> -NH	2.0	−3.8	−5.8	0.87	9.4	41	3.3	TTFQx-T1	TA @180 °C	[96]
tPDI <sub>2</sub> N-benzyl	2.4	−3.6	−6.0	0.99	14.1	42	5.8	QX1	TA @180 °C	[98]
tPDI <sub>2</sub> N-benzylF	2.4	−3.6	−6.0	0.96	15.1	41	5.8	QX1	TA @180 °C	[98]
tPDI <sub>2</sub> N-benzylF5	2.4	−3.6	−6.0	0.96	14.4	40	5.5	QX1	TA @180 °C	[98]
tPDI <sub>2</sub> N-EH	2.2	−3.7	−5.9	0.95	15.3	43	6.6	PTB7-Th	0.25% DIO	[99]
tPDI <sub>2</sub> N-EH	2.2	−3.7	−5.9	1.04	9.4	59	5.7	BDT-QX	3% DPE	[100]
tPDI <sub>2</sub> N-EH	2.2	−3.7	−5.9	1.09	11.7	51	6.6	QX3	As-cast	[101]
tPDI <sub>2</sub> N-EH	2.2	−3.7	−5.9	1.04	10.5	58	6.4	QX1	ZnO/PDIN-hex	[102]
tPDI <sub>2</sub> N-EH	2.2	−3.7	−5.9	1.21	8.2	55	5.5	PTQ10	Toluene + 1% DPE	[85]
PDI <sub>2</sub> dimers for ternary OPVs										
tPDI <sub>2</sub> N-Hex	2.2	−3.7	−5.9	0.87	14.3	71	8.5	PBDB-T	PBDB-T: PC <sub>61</sub> BM: tPDI <sub>2</sub> N-Hex	[103]
tPDI <sub>2</sub> N-EH	2.2	−3.7	−5.9	1.24	7.7	40	3.8	PTQ10	PTQ10: tPDI <sub>2</sub> N-EH: PDI-EDOT-PDI	[85]
tPDI <sub>2</sub> N-EH	2.2	−3.7	−5.9	0.86	13.2	69	7.9	PPDT2FBT	FBT: PC <sub>61</sub> BM: tPDI <sub>2</sub> N-EH	[104]
PDI <sub>2</sub> dimers for indoor OPVs										
tPDI <sub>2</sub> N-EH	2.2	−3.7	−5.9	0.84	66.8 × 10 <sup>-3</sup>	51	9.6	PPDT2FBT	@1000 lux (warm LED)	[105]
tPDI <sub>2</sub> N-EH	2.2	−3.7	−5.9	1.07	139 × 10 <sup>-3</sup>	48	11.7	PTQ10	@2000 lux (warm LED)	[85]
tPDI <sub>2</sub> N-EH	2.2	−3.7	−5.9	0.72	167 × 10 <sup>-3</sup>	73	15.5	PPDT2FBT	@2000 lux (warm LED)	[104]
Asymmetric dimers										
PDI-DPP-IQ	1.5	−3.7	−5.2	0.75	2.5	42	0.8	P3HT	5 min SVA	[82]
PDI-DPP-BTXI	1.6	−3.7	−5.3	0.95	3.8	31	1.1	PTB7-Th	10 min SVA	[106]
NPDI-DPP-SePDI	1.6	−3.7	−5.3	0.76	2.7	38	0.8	PTB7-Th	5 min SVA	[107]

### 3.1. N-Annulated PDI Electron Acceptors (PDI-Core-PDI)

#### 3.1.1. PDI-DPP-PDI

The organic dye diketopyrrolopyrrole (DPP) was utilized as a core between two PDI units. DPP-based small molecules have been reported to organize in the film with solvent vapor annealing (SVA) treatment, which was a motivation for its use [108]. DPP is a relatively weaker acceptor than PDI, which creates a unique all-acceptor-based, push-pull system with strong panchromatic light absorption (the chemical structure of the DPP core is illustrated in Figure 6b). McAfee et al. [84] demonstrated the facile synthesis of PDI-DPP-PDI using direct-heteroarylation (DHA) cross-coupling methods. The optical absorption spectra of the PTB7-Th:PDI-DPP-DPI blend showed strong light absorption from 400 to 800 nm with an increase at 586 nm upon SVA treatment for 2–5 min (Figure 5c), which is attributed to the crystallization of the PDI-DPP-PDI molecule. A PCE of 5.6% ( $V_{oc} = 0.98$  V;  $J_{sc} = 11.32$  mA/cm<sup>2</sup>; FF = 50.1%) was achieved using chloroform SVA treatment for 2.5 min. The  $J$ - $V$  curves (Figure 6d) and EQE spectra (Figure 6e) of the OPV devices with and without SVA treatment of the photoactive layer show that the SVA treatment led to a significant increase in photocurrent generation in the visible region.

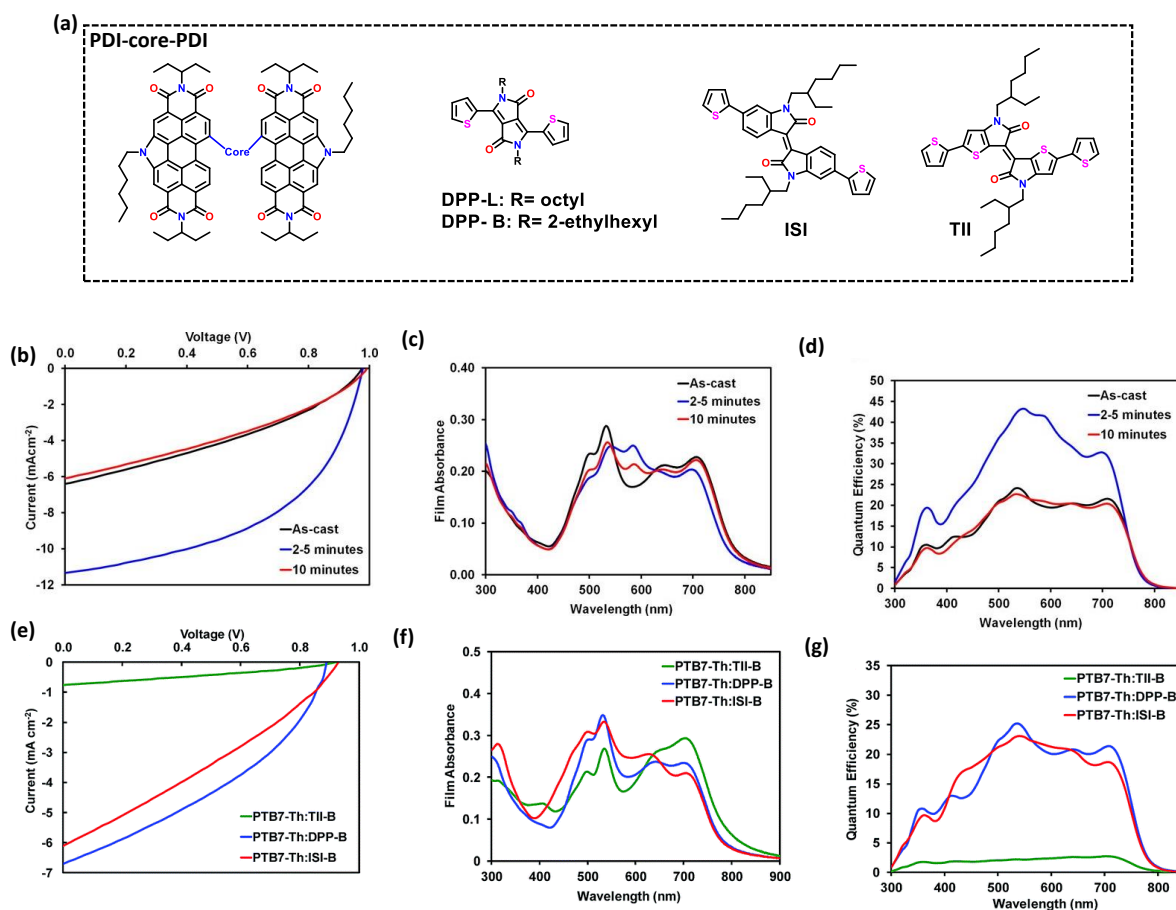


**Figure 6.** (a) General chemical structure of the PDI-Core-PDI framework and chemical structure of DPP-L (R = Octyl), DPP-B (R = 2-ethylhexyl), ISI-B, and TII-B dye cores used in PDI-core-PDI dimers. (b) Device  $J$ - $V$  curves, (c) film UV-Vis absorption spectra, and (d) device EQE of PTB7-Th:PDI-DPP-PDI blends before and after SVA. (e) Device  $J$ - $V$  curves, (f) film UV-Vis absorption spectra, and (g) device EQE of PTB7-Th:PDI-X-PDI blends where X = TII-B, DPP-B, ISI-B [84,86,87]. (b–d), and (e–g) reproduced with permissions from [84],[86] respectively. Copyright 2017 American Chemical Society and 2017 Royal Society of Chemistry.

Following this, McAfee et al. [87] demonstrated a multigram synthesis of PDI-DPP-PDI, and the NFA molecule was blended with four different BDT-based donor polymers (PTB7-Th, PBDB-T, J61, and TTFQx-T1) to identify best donor/acceptor pairings. The best OPV device performance was obtained using the donor polymer PTB7-Th, providing a PCE of 6.2% ( $V_{oc} = 0.98$  V;  $J_{sc} = 14.52$  mA/cm<sup>2</sup>; FF = 44%). The pairing with TTFQx-T1 provided devices with a slightly lower PCE of 5.7% ( $V_{oc} = 1.02$  V;  $J_{sc} = 11.53$  mA/cm<sup>2</sup>; FF = 49%). Pairing with PBDB-T and J61 resulted in device performance drops, demonstrating PCEs of 2.3% ( $V_{oc} = 1.0$  V;  $J_{sc} = 5.77$  mA/cm<sup>2</sup>; FF = 40%) and 3.1% ( $V_{oc} = 0.99$  V;  $J_{sc} = 6.66$  mA/cm<sup>2</sup>; FF = 48%), respectively. Consistent for all blends was the use of a short SVA treatment to crystallize the PDI-DPP-PDI acceptor and boost the OPV performance.

Further developing this type of NFA, McAfee et al. [86] investigated the role of other dye-based cores, including DPP with branched side chains (DPP-B), isoindigo (ISI-B), and thienylisoindigo (TII-B) (Figure 6a,b). The compounds were paired with the donor polymer, PTB7-Th, devices were fabricated, and the OPV performance was measured. The devices based on TII-B, DPP-B, and ISI-B showed much lower performances of 0.4% ( $V_{oc} = 0.93$  V;  $J_{sc} = 1.09$  mA/cm<sup>2</sup>; FF = 34%), 2.9% ( $V_{oc} = 0.97$  V;  $J_{sc} = 6.0$  mA/cm<sup>2</sup>; FF = 50%), and 2.6% ( $V_{oc} = 1.03$  V;  $J_{sc} = 6.97$  mA/cm<sup>2</sup>; FF = 37%), respectively, (Figure 6g) compared to devices based on the parent PDI-DPP-PDI NFA. This work highlights the importance of dye core selection, specifically the use of DPP, and the role of side-chain engineering in which linear side chains on the DPP core enable the formation of crystalline domains in the BHJ and deliver the best OPV performance.

### 3.1.2. Boron Difluoride Formazanate Non-Fullerene Acceptor

Cann et al. explored the optoelectronic properties of N-annulated PDI NFA dimers containing different cores connected to the PDIs with acetylene linkers [109]. They found that by linking the PDI units to the dye cores through acetylene linkers, steric interactions are minimized. This allows for strong electronic communication between the PDIs and the dye cores, leading to intense panchromatic optical absorption. Motivated by this work and with a goal to develop narrow-bandgap PDI-based NFAs, the formazanate (BF<sub>2</sub>fz) chromophore was investigated as an electron-deficient core with strong light absorption [110]. A new NFA (PDI-BF<sub>2</sub>fz-PDI), comprised of a BF<sub>2</sub>fz core acetylene-linked to N-annulated PDI endcaps, was introduced by Koeing et al. [88]. (Figure 7a). Figure 7b shows the UV-Vis absorption spectra of PDI-BF<sub>2</sub>fz-PDI films before and after a 5 min chloroform SVA treatment. Prior, SVA treatment was proven to induce crystallization of DPP-containing PDIs, leading to significant changes in optical absorption [82]. After the 5 min chloroform SVA treatment, a red shift of 150 nm in the onset of absorption was observed in both neat and blend films (Figure 7b,c). Proof-of-concept OPV devices were fabricated to evaluate the capabilities of the new molecule as an NFA. The PDI-BF<sub>2</sub>fz-PDI acceptor was used as a third component in a ternary blend composed of FBT (donor polymer) and PC<sub>61</sub>BM (fullerene acceptor) with a blend ratio of (1:1:0.5 *w/w*) and a 10 mg/mL total concentration. OPV devices with active layers treated under chloroform SVA conditions showed enhanced photovoltaic performance compared to as-cast devices. The PCEs doubled due to  $J_{sc}$  enhancement (Figure 7d,e). Surface morphologies (as determined by AFM) showed distinct differences between the as-cast and SVA-treated blend films. The root mean square surface roughness of the films increased from 1.9 nm for the as-cast films to 4.8 nm for the SVA-treated films (Figure 7f). The enhanced performance in OPV devices was attributed to the aggregation of PDI-BF<sub>2</sub>fz-PDI into phase-separated domains rather than crystallization.

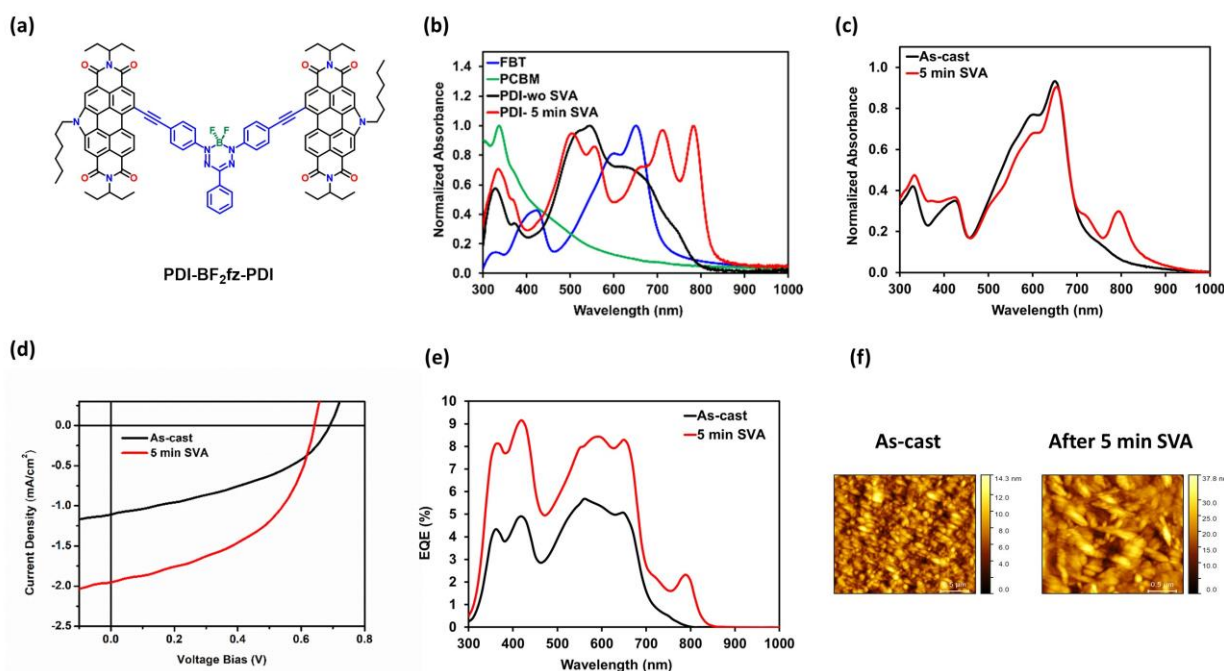


**Figure 7.** (a) Chemical structures of the PDI-BF<sub>2</sub>fz-PDI acceptor, (b) UV-Vis absorption spectra of neat films before and after chloroform SVA, (c) UV-Vis absorption spectra, (d) device *J*-*V* curves, (e) device EQE, and (f) AFM images comparing the effects of SVA using chloroform on ternary blend OPV devices with FBT:PDI-BF<sub>2</sub>-PDI:PC<sub>61</sub>BM (1:1:0.5) active layers [88]. (b–f) reproduced with permission from [88]. Copyright 2020 Royal Society of Chemistry.

### 3.1.3. PDI-Thiophene-PDI

Lowering the electron affinity (i.e., raising the LUMO energy level) [31] of PDI is desired to increase the operating  $V_{oc}$  in OPV devices by maximizing the energy gap between the HOMO of the donor and the LUMO of the acceptor. The use of electron-rich thiophene cores (donor) with the PDI dye (acceptor), thus applying the donor–acceptor (D–A) strategy, was carried out to precisely tune energy levels and optical absorption. N-annulated PDI dimers bearing various thiophene linkers (PDI-core-PDI) were reported by our group (Figure 8a) [89–93]. Hendsbee et al. demonstrated that the use of thiophene or bithiophene as the core destabilized the LUMO energy levels to 3.47 and 3.54 eV and electrochemical bandgaps of 2.22 and 2.04 eV, respectively, relative to the parent N-hexyl PDI dimer (tPDI<sub>2</sub>N-Hex; LUMO energy level = 3.76 eV; electrochemical band gap = 2.23 eV) [89]. The PDI NFAs with thiophene cores were paired with the PTB7-Th donor polymer to deliver OPV devices with high  $V_{oc}$  values above 1 V. However, the inability of the NFAs to form crystalline domains when compared to tPDI<sub>2</sub>N-Hex resulted in poor device performances. To tackle this design drawback, thiophene core fusion was proposed to enhance the PDI self-assembly and increase the acceptor domain crystallinity. Laventure et al. developed a fused, thiophene-based PDI acceptor (F-NPDI<sub>2</sub>), which lead to devices with a higher  $V_{oc}$  (ca. 1.1 V) [90] and improved device PCEs.

Further chemical modification of the thiophene-based dimers was introduced by Welsh et al., using dithienophosphole and borane incorporation [91,92]. *P*-phenyl dithienophosphole oxide (Th<sub>2</sub>PO) was used as a core, providing the NFA PDI-Th<sub>2</sub>PO-PDI (Figure 8a). Again, OPV devices based on this NFA and the PBDB-T donor polymer had high  $V_{oc}$  values (1.1 V), but only moderate PCE values (ca. 2.3%). In contrast, incorporating boron into the molecular framework, namely, PDI-Th<sub>2</sub>B-PDI, led to a twisting of the structure [92]. With the addition of the borane unit, the electrochemical bandgap increased from 2.12 eV for PDI-Th<sub>2</sub>PO-PDI to 2.20 eV in PDI-Th<sub>2</sub>B-PDI. OPV devices using this NFA, and the medium-gap donor polymer TTFQx-T1(QX1) provided a PCE of 1.8% ( $V_{oc}$  = 1 V;  $J_{sc}$  = 5.3 mA/cm<sup>2</sup>; FF = 33%) for the devices with as-cast active layers. With thermal annealing of the active layers for 10 min

at 180 °C, PCEs increased to 2.3% ( $V_{oc} = 1$  V;  $J_{sc} = 6.9$  mA/cm<sup>2</sup>; FF = 33%). Use of a 5% diphenyl ether solvent additive (DPE) during photoactive film formation, in addition to thermal annealing for 10 min at 180 °C, led to a PCE of ~3.9% ( $V_{oc} = 1.0$  V;  $J_{sc} = 9.3$  mA/cm<sup>2</sup>; FF = 37%), nearly double that of the phosphine oxide analogue (Figure 8). For the PDI-Th<sub>2</sub>B-PDI, the overlap of the thiophene  $\pi^*$  orbitals and the boron P<sub>z</sub> orbital [111] helps to stabilize the LUMO, while for PDI-Th<sub>2</sub>PO-PDI, the LUMO is stabilized through the overlap of the bithiophene  $\pi^*$  orbital and exocyclic P—R  $\sigma^*$  orbitals [112]. Both have a higher electron affinity than the parent bithiophene analogue (PDI-Th<sub>2</sub>-PDI), but they have different geometries due to the fused planar structure of Th<sub>2</sub>PO and the trigonal structure of Th<sub>2</sub>B, providing a comparison of the effect of molecule shape on device characteristics.

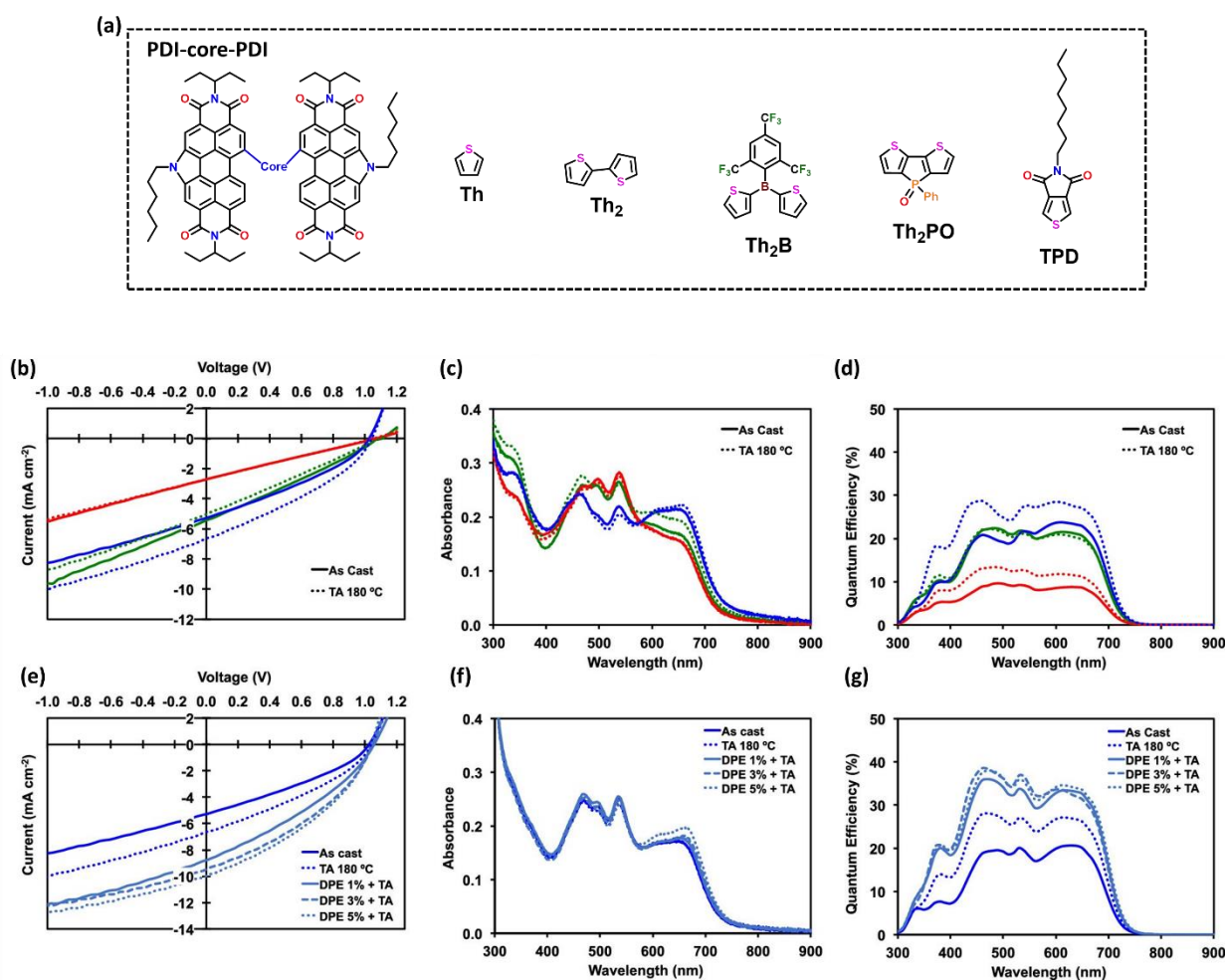


**Figure 8.** (a) Chemical structure of the PDI-Core-PDI framework and various thiophene core linkers, (b) device  $J$ - $V$  curves, (c) UV-Vis absorption spectra, and (d) device EQE for best devices with as-cast and thermally annealed TTFQx-T1/acceptor active layers (green = TTFQx-T1/PDI-Th<sub>2</sub>-PDI; red = TTFQx-T1/PDI-Th<sub>2</sub>PO-PDI; blue = TTFQx-T1/PDI-Th<sub>2</sub>B-PDI). (e) device  $J$ - $V$  curves, (f) UV-Vis absorption spectra, and (g) device EQE for best devices with as-cast, thermally annealed, and DPE additive processed TTFQx-T1/PDI-Th<sub>2</sub>B-PDI active layers [92]. (b–g) reproduced with permission from [92]. Copyright 2019 American Chemical Society.

Another thiophene building block, thieno[3,4-*c*]pyrrole-4,6-dione (TPD), was used as a core to create the NFA PDI-TPD-PDI [93] (Figure 8). TPD is a commonly used building block for constructing organic photoactive materials with an electron-deficient aromatic system, a site for side-chain engineering, and activated CH bonds for facile functionalization using DHA methods [113]. The PDI-TPD-PDI NFA molecule can be considered a hybrid structure of our previously designed NFAs: PDI-DPP-PDI [86] and tPDI<sub>2</sub>N-Hex [81]. The use of TPD

was to provide enough steric bulk between the two PDI units to twist the structure and prevent significant aggregation, mimicking the effect in tPDI<sub>2</sub>N-Hex while being electron-deficient, maintaining a low-lying LUMO energy level, and having a linear octyl chain (such as within PDI-DPP-PDI) to enable the molecule to self-organize within the film. The introduction of the TPD core did not have large impact on the ionization potential and electron affinity values (IP = 5.9 eV, EA = 3.7 eV, and  $E_{elec} = 2.2$  eV) relative to tPDI<sub>2</sub>N-Hex with no core. A PCE of ~3.28% ( $V_{oc} = 1.05$  V;  $J_{sc} = 7.40$  mA/cm<sup>2</sup>; FF = 42%) was realized for OPV devices using the donor polymer PDBD-T with PDI-TPD-PDI. The use of the DPE solvent additive during BHJ film formation, which induced phase separation, was key.

### 3.2. Tetramers

Indacenodithiophene (IDT) is a rigid, rod-like organic conjugated building block that has been used to create one of the most successful NFAs to date, namely, ITIC [56,114]. Payne et al. used IDT as a core for four PDI units (synthesized via a 4-fold DHA coupling method), providing the tetrameric NFA IDT-NPDI<sub>4</sub> (Figure 9a), which exhibited with a pseudo-butterfly structure [94]. The ease of functionalization of the thiophene-based core provides a simple synthetic pathway towards tetrameric PDIs. The UV-Vis absorption spectra of IDT, NPDI building blocks, and the IDT-NPDI<sub>4</sub> NFA as thin films are shown in Figure 9b. The absorption spectrum of the IDT-NPDI<sub>4</sub> NFA is dominated by the four PDIs, which have higher-energy bands attributed to the IDT core.

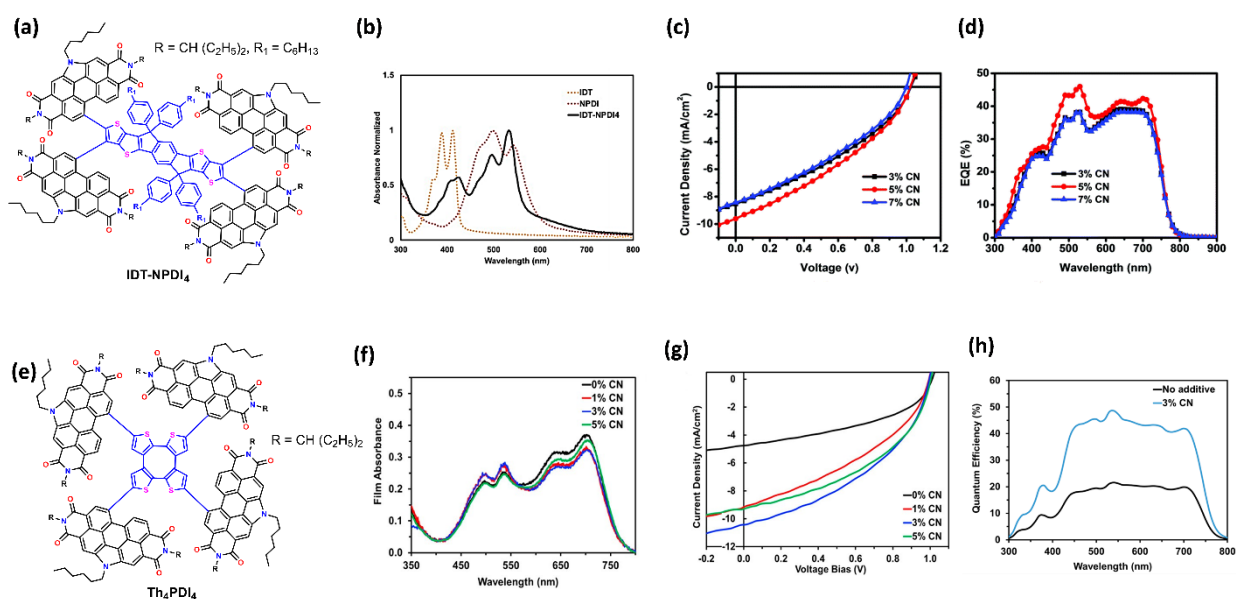


**Figure 9.** (a) Chemical structure of IDT-NPDI<sub>4</sub>, (b) UV-Vis absorption spectra, (c) device  $J$ - $V$  curves, (d) device EQE of the PTB7:IDT-NPDI<sub>4</sub> photoactive layers processed with various chloronaphthalene (CN, additive) percentages. (e) Chemical structure of Th<sub>4</sub>-PDI<sub>4</sub>, (f) UV-Vis absorption spectra, (g) device  $J$ - $V$  curves, (h) device EQE of the PTB7:Th<sub>4</sub>-PDI<sub>4</sub> photoactive layers with various CN percentages [94,95]. (b-d) and (f-h) reproduced with permissions from [94,95], respectively. Copyright 2018 Royal Society of Chemistry and 2019 American Chemical Society.

To test the validity of IDT-NPDI<sub>4</sub> as an NFA, OPV devices were fabricated by blending it with the PTB7-Th donor polymer. Various amounts of a chloronaphthalene (CN) additive of 3%, 5%, and 7% in chlorobenzene, used during BHJ film formation, achieved device PCEs of 3.03% ( $V_{oc} = 1.03$  V;  $J_{sc} = 8.53$  mA/cm<sup>2</sup>; FF = 35%), 3.41% ( $V_{oc} = 1.02$  V;  $J_{sc} = 9.62$  mA/cm<sup>2</sup>; FF = 35%), and 2.9% ( $V_{oc} = 1.00$  V;  $J_{sc} = 8.44$  mA/cm<sup>2</sup>; FF = 34%), respectively. High  $V_{oc}$  values >1 were obtained with modest  $J_{sc}$  values (8–10 mA/cm<sup>2</sup>) but poor FFs (Figure 9c). The contribution of the IDT-NPDI<sub>4</sub> NFA to light harvesting was confirmed by EQE measurements (Figure 9d).

A follow-up work by Koenig et al., which used a less rigid  $\pi$ -conjugated cyclooctatetrathiophene (Th<sub>4</sub>) core, introduced the tetrameric NFA Th<sub>4</sub>PDI<sub>4</sub> (Figure 9e) [95]. The new NFA design was proposed to provide a different molecular shape when compared with IDT-NPDI<sub>4</sub>; this might be the reason behind the poor FFs obtained. Testing the viability of Th<sub>4</sub>PDI<sub>4</sub> as an NFA, OPV devices were fabricated by pairing it with a PTB7-Th donor polymer. Figure 9e shows the complementary absorption of Th<sub>4</sub>PDI<sub>4</sub> (400–600 nm) and PTB7-Th (600–750 nm). A device PCE of 2.2% ( $V_{oc}$  = 1.01 V;  $J_{sc}$  = 5.1 mA/cm<sup>2</sup>; FF = 42%) was obtained for devices with as-cast active layers. The addition of various amounts of CN additive (1%, 3%, and 5% CN) during the BHJ film formation enhanced the device PCEs to 3.61% ( $V_{oc}$  = 0.98 V;  $J_{sc}$  = 9.5 mA/cm<sup>2</sup>; FF = 39%), 4.52% ( $V_{oc}$  = 0.99 V;  $J_{sc}$  = 10.6 mA/cm<sup>2</sup>; FF = 43%), and 4.16% ( $V_{oc}$  = 1.00 V;  $J_{sc}$  = 9.3 mA/cm<sup>2</sup>; FF = 45%), respectively (Figure 9g). EQE measurements of devices with and without the 3% CN additive showed a significant enhancement of the photocurrent generation when additives were used for processing the BHJs (Figure 9h). While the IDT-NPDI<sub>4</sub> and Th<sub>4</sub>PDI<sub>4</sub> tetrameric NFAs only provided modest PCEs, facile synthesis using DHA methods opens the possibility for a larger number of tetrameric structures to be designed and synthesized for probing structure–function relationships.

### 3.3. Side Chain Engineering of Perylene Diimide Dimers

#### 3.3.1. Benzyl Side Chains

We have extensively studied the effect of side-chain engineering N-annulated PDI dimers on OPV device performance [81,83,96,99,103,105] through the functionalization of the pyrrolic N-atoms. Nazari et al. developed three PDI dimers using benzyl-based moieties at the pyrrolic N-atoms. Benzyl, 4-fluorobenzyl, and pentafluorobenzyl were used as side chains to form the compounds tPDI<sub>2</sub>N-benzyl (1), tPDI<sub>2</sub>N-benzylF (2) and, tPDI<sub>2</sub>N-benzylF<sub>5</sub> (3), shown in Figure 10a [98]. The UV–Vis absorption spectra of the neat PDI films and BHJ blended films (with either donor polymer PTB7-Th or QX1) are shown in Figure 10b,c and exhibit complementary optical absorption. The photovoltaic characteristics of (1), (2), and (3) were evaluated by blending them with PTB7-Th or QX1 for BHJ layer formation. OPV devices with PTB7-Th: NFA and QX1: NFA BHJ blends demonstrated a similar trend in terms of photovoltaic characteristics (Figure 10d,e). The PTB7-Th:1 blend provided the best device performance, demonstrating a PCE of 5.7% ( $V_{oc}$  = 0.96 V;  $J_{sc}$  = 11.7 mA/cm<sup>2</sup>; FF = 51%) compared to PCEs of 4.9% ( $V_{oc}$  = 0.90 V;  $J_{sc}$  = 11.0 mA/cm<sup>2</sup>; FF = 49%) and 4.2% ( $V_{oc}$  = 0.89 V;  $J_{sc}$  = 10.2 mA/cm<sup>2</sup>; FF = 47%) for devices based on the PTB7-Th:2 and PTB7-Th:3 BHJ blends, respectively. Switching to the QX1 polymer donor resulted in higher device PCEs yet similar metrics, regardless of the acceptor used: QX1:1 (PCE = 5.8%;  $V_{oc}$  = 0.99 V;  $J_{sc}$  = 14.1 mA/cm<sup>2</sup>; FF = 42%), QX1:2 (PCE = 5.8%;  $V_{oc}$  = 0.96 V;  $J_{sc}$  = 15.1 mA/cm<sup>2</sup>; FF = 41%), and QX1:3 (PCE = 5.5%;  $V_{oc}$  = 0.96 V;  $J_{sc}$  = 14.4 mA/cm<sup>2</sup>; FF = 40%). It is important to note that the introduction of F-atoms into the benzyl side chains stabilizes the frontier molecular orbital energy levels, which directly correlate to a drop in  $V_{oc}$  values for the OPV devices.

#### 3.3.2. Alkyl Side Chains

The N-alkyl chain modification of twisted PDI dimers and its effect on OPV device performance were first reported by Hendsbee et al. (Figure 11a) [81,99]. First, ethyl-(7b) and hexyl-functionalized (7 or tPDI<sub>2</sub>N-Hex) N-annulated PDI dimers provided device PCEs of 5.5% and 5.1%, respectively, when paired with a PTB7-Th donor polymer. Using the P3TEA donor polymer with PDI NFA 7b led to the higher device PCE of 7.5% ( $V_{oc}$  = 1.13 V;  $J_{sc}$  = 11 mA/cm<sup>2</sup>; FF = 61%), as shown in Figure 11b–d. The promising photovoltaic performance coupled with the simple, scalable, and reproducible synthesis encouraged us to further optimize these PDI derivatives and use green solvent processing methods [99]. A series of eight different PDI dimers functionalized with alkyl chains with lengths ranging from linear methyl (C1) to octyl (C8) and the branched alkyl chain 2-ethylhexyl (C8b) were synthesized and characterized, and their use in OPV devices

was evaluated. Inverted-type OPV devices were fabricated with BHJ blends comprising PTB7-Th and each PDI NFA, all processed from the green solvent 2Me-THF. It was found that regardless of alkyl chain length, comparable photovoltaic performances were achieved. Ethyl- and hexyl-functionalized PDI dimers gave good device PCEs of 4.8% ( $V_{oc} = 0.95$  V;  $J_{sc} = 11.4$  mA/cm<sup>2</sup>; FF = 43%) and 5.5% ( $V_{oc} = 0.96$  V;  $J_{sc} = 12.1$  mA/cm<sup>2</sup>; FF = 45%). The branched 2-ethylhexyl side-chain functionalized PDI dimer (**C8b**, tPDI<sub>2</sub>N-EH) provided the best device performance with a PCE of 6.5% ( $V_{oc} = 0.96$  V;  $J_{sc} = 15.4$  mA/cm<sup>2</sup>; FF = 43%) (Figure 11e–g). From these results, we conclude that while the length of the side chain does not matter significantly, the use of a longer and branched side chain produces a PDI NFA that performs best in OPV devices.

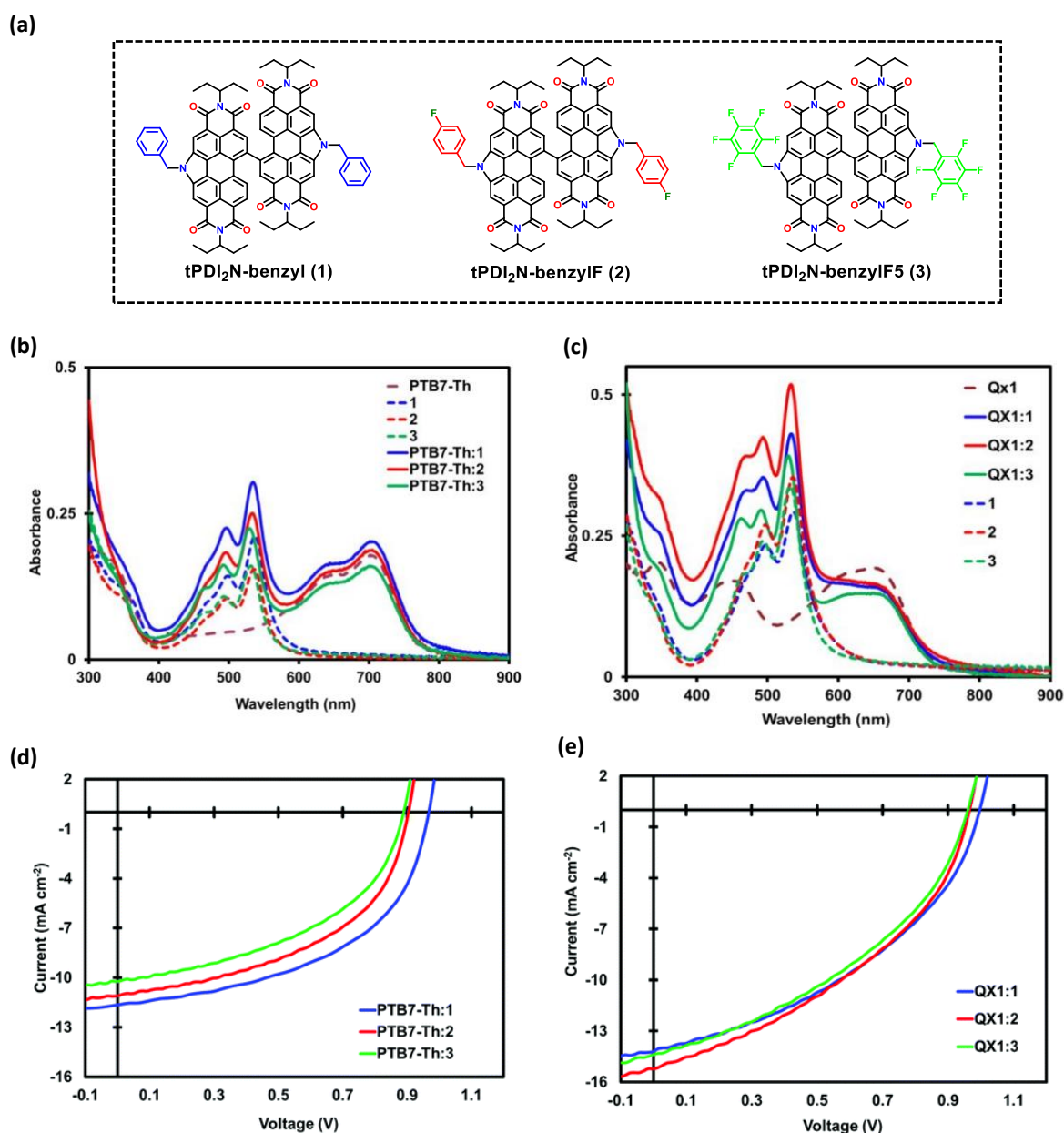


**Figure 10.** (a) Chemical structure of tPDI<sub>2</sub>N-benzyl (1), tPDI<sub>2</sub>N-benzylF (2), and tPDI<sub>2</sub>N-benzylF5 (3), (b) UV-Vis absorption spectra of the neat PTB7-Th, neat PDI 1–3, and BHJ blends, (c) UV-Vis absorption spectra of the neat QX1, neat PDI 1–3, and BHJ blends, (d) device  $J$ - $V$  curves of PTB7-Th: PDI 1–3 blends (1:1), and (e) device  $J$ - $V$  curves of QX1: PDI 1–3 blends (1:1.5) [98]. (b–e) reproduced with permission from [98]. Copyright 2018 Royal Society of Chemistry.

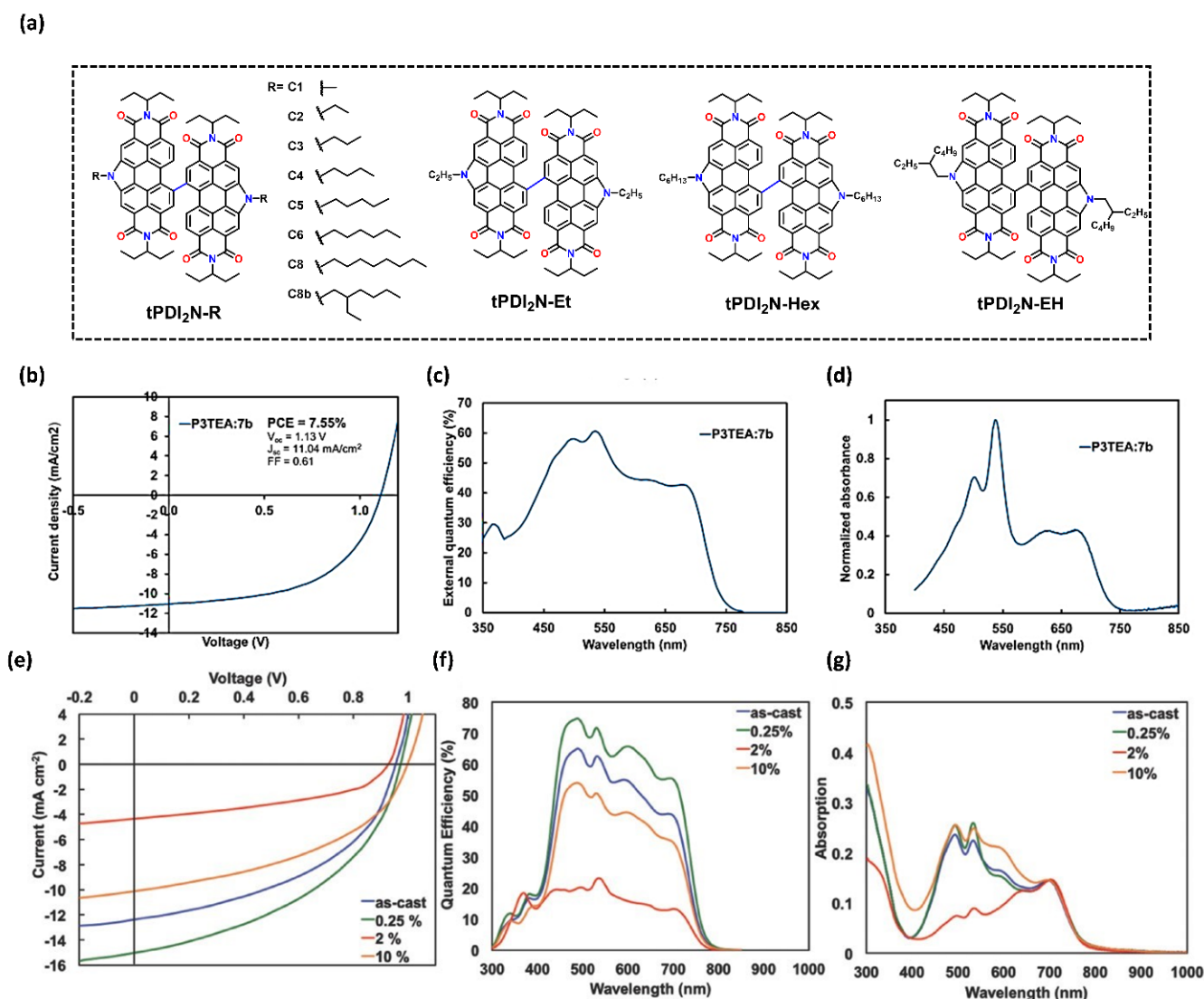


**Figure 11.** (a) Chemical structure of PDI dimers with various alkyl side chains (b) device  $J$ - $V$  curves, (c) device EQE, and (d) UV-Vis absorption spectra of OPV devices based on a blend of P3TEA and **7b** processed from 1,3,5-trimethyl benzene with 1,8-octane dithiol additive [81]. (e) device  $J$ - $V$  curves, (f) device EQE, and (g) UV-Vis absorption spectra of OPV devices based on PTB7-Th:**C8b** blend films from 2Me-THF, as-cast and with different 1,8-diiodooctane (DIO) concentrations ( $v/v\%$ ) [99]. Note that **7b** = tPDI<sub>2</sub>N-Hex and **C8b** = tPDI<sub>2</sub>N-EH. (b–d), and (e–g) are reproduced with permissions from [81,99], respectively. Copyright 2016 Royal Society of Chemistry and 2018 Wiley.

As mentioned prior, the insertion of acetylene units as spacers in tPDI<sub>2</sub>N-Hex was proposed as a strategy to control the steric hindrance between the PDI subunits [97]. Adding one acetylene spacer led to partially twisted dimer when compared to tPDI<sub>2</sub>N-Hex, which is highly twisted. Adding two acetylene spacers rendered the PDI subunits coplanar. However, acetylene spacers were found to reduce the material's solubility in organic solvents and thus induced strong aggregation in both solution and thin films. The latter led to a dramatic deterioration in OPV device performance (PCE = 1.3%,  $V_{oc}$  = 0.95 V;  $J_{sc}$  = 4.4 mA/cm<sup>2</sup>; FF = 32%) compared to the devices using the parent tPDI<sub>2</sub>N-Hex (PCE = 5.2%,  $V_{oc}$  = 0.96 V;  $J_{sc}$  = 11.5 mA/cm<sup>2</sup>; FF = 47%). Thus, in-line with the current literature on PDI-based NFAs, molecular-based NFAs using PDI subunits perform better in OPV devices when the structure has non-planar (i.e., twisted) arrangements of the PDIs.

### 3.3.3. Versatile Applications of t-PDI<sub>2</sub>N-Hex and t-PDI<sub>2</sub>N-EH in OPVs Ternary Approach, Slot-Die (SD)-Coated Active Layers and Indoor Light Harvesting

The tPDI<sub>2</sub>N-Hex NFA was introduced as a third component in PBDB-T:PC<sub>61</sub>BM BHJ blends to fabricate ternary OPVs. All the active layers were processed in air from chlorobenzene, using 3% DIO as solvent additive. It was observed that 10 wt.% tPDI<sub>2</sub>N-Hex was enough to enhance the device PCE from 8.1% for the binary blend (PBDB-T:PC<sub>61</sub>BM) to 8.8% for the ternary blend (PBDB-T:PC<sub>61</sub>BM:tPDI<sub>2</sub>N-Hex). The device performance enhancement was mainly due to an increase in the  $V_{oc}$  from 0.80 V for the binary blend to 0.87 V for the ternary blend. tPDI<sub>2</sub>N-Hex has optical absorption from 400 to 600 nm, complementing the optical absorption of the PBDB-T:PC<sub>61</sub>BM blend.

Owing to the high  $V_{oc}$  (1.0 V) values and the strong optical absorption in the visible range (400–650 nm), OPV devices using the tPDI<sub>2</sub>N-EH NFA were evaluated for indoor light harvesting applications [105]. BHJ blends were processed from *o*-xylene and made use of the FBT donor polymer. Inverted-type OPV devices provided a PCE of 6.5% ( $V_{oc} = 1.03$  V;  $J_{sc} = 11.9$  mA/cm<sup>2</sup>; FF = 53%) under 1 sun illumination with spin-coated BHJs (Figure 12a). With slot-die coating the BHJs, the inverted-type OPV devices provided a PCE of 4.6% ( $V_{oc} = 1.02$  V;  $J_{sc} = 9.5$  mA/cm<sup>2</sup>; FF = 48%). The drop in PCE observed in the transition from spin coating to slot-die coating the BHJs was attributed to the slow drying time associated with the slot-die coating, which allowed for unfavorable phase separation. Under low-light illumination (cold and warm white LED source; 600 lux), OPV devices with slot-die-coated BHJs had a PCE of 9.2% ( $V_{oc} \approx 0.82$  V;  $J_{sc} \approx 40.3$   $\mu$ A/cm<sup>2</sup>; FF  $\approx$  51%) and an output power of  $P_{out} \approx 16.6$   $\mu$ W/cm<sup>2</sup>, as shown in Figure 12b,c. Compared to OPV devices using other acceptors (PC<sub>60</sub>BM, ITIC-M, and ITIC-F) and a reference Si diode, the devices based upon tPDI<sub>2</sub>N-EH had the highest  $V_{oc}$  values and PCEs second to only the fullerene-based systems. These results demonstrated how N-annulated PDI-based NFAs have utility for indoor photovoltaic applications.

A follow-up work by Farahat et al. introduced OPVs based on the FBT:PC<sub>61</sub>BM:tPDI<sub>2</sub>N-EH (PDI) ternary blend for indoor light harvesting [104]. In this study, the PDI acceptor was added to the FBT:PC<sub>61</sub>BM blend with content at 10–50% of the total concentration (Figure 13a–c). Optimized OPV devices with spin-coated BHJs (ternary blend ratio of 1:1.2:0.3) achieved a PCE of 7.9% ( $V_{oc} = 86$  V;  $J_{sc} = 13.4$  mA/cm<sup>2</sup>; FF = 68%) compared to a PCE of 7% ( $V_{oc} = 76$  V;  $J_{sc} = 12.5$  mA/cm<sup>2</sup>; FF = 73%) for devices using a binary BHJ blend (i.e., only FBT:PC<sub>61</sub>BM). Using PEIE/ZnO as the electron transport layer (ETL) instead of ZnO provided similar device performance but with more consistency and reproducibility (PCE = 7.4% for binary and PCE = 7.9% for ternary). Under the optimized processing conditions, OPV devices with slot-die-coated binary blend BHJs had a drop in performance, demonstrating a PCE of 6.8% ( $V_{oc} = 78$  V;  $J_{sc} = 12.3$  mA/cm<sup>2</sup>; FF = 71%) when compared to their spin-coated counterparts. On the other hand, OPV devices with slot-die-coated ternary blend BHJs retained performance (PCE = 7.7%;  $V_{oc} = 86$  V;  $J_{sc} = 13$  mA/cm<sup>2</sup>; FF = 69%, Figure 13d) when compared to their spin-coated counterparts.

The optical absorption spectra of the FBT:PC<sub>61</sub>BM and FBT:PC<sub>61</sub>BM:PDI blended films exhibited a strong visible light absorption which directly overlaps with the emission of indoor lights (Figure 13e,f). Under low-light LED illumination [ca. 2000 lux (568  $\mu$ W/cm<sup>2</sup> respectively)], OPV devices with slot-die-coated binary or ternary BHJs achieved PCEs of 12% ( $V_{oc} = 0.63$  V;  $J_{sc} = 154$   $\mu$ A/cm<sup>2</sup>; FF = 70%) and 14% ( $V_{oc} = 72$  V;  $J_{sc} = 153$   $\mu$ A/cm<sup>2</sup>; FF = 72%), respectively, as shown in Figure 13g. Devices with spin-coated BHJs under the same conditions achieved PCEs of 13.1% ( $V_{oc} = 0.63$  V;  $J_{sc} = 162$   $\mu$ A/cm<sup>2</sup>; FF = 73%) and 15.5% ( $V_{oc} = 72$  V;  $J_{sc} = 167$   $\mu$ A/cm<sup>2</sup>; FF = 73%), respectively, as shown in Figure 13h.

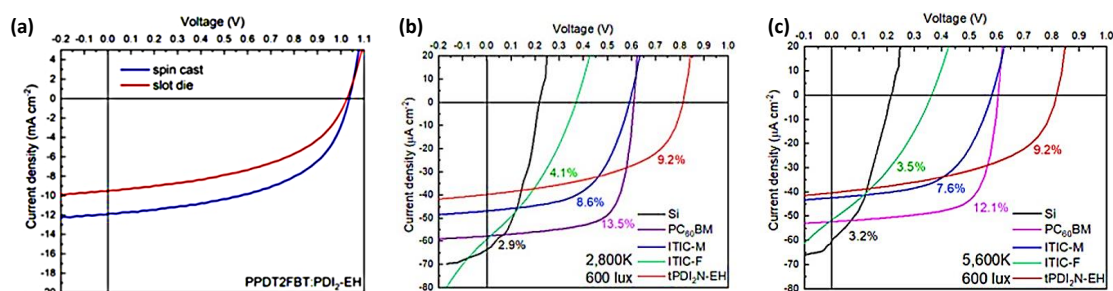


**Figure 12.** (a) Device  $J$ - $V$  curves of the slot-die vs. spin-coated active layers based on PPDT2FBT (FBT):tPDI<sub>2</sub>N-EH under 1 sun illumination, (b,c)  $J$ - $V$  curves of the slot-die-coated active layers based on different acceptors paired with FBT under 600 lux warm white 2800 K LED and cold white 5600 K LED, respectively [105]. (a–c) Reproduced with permission from [105]. Copyright 2019 American Chemical Society.

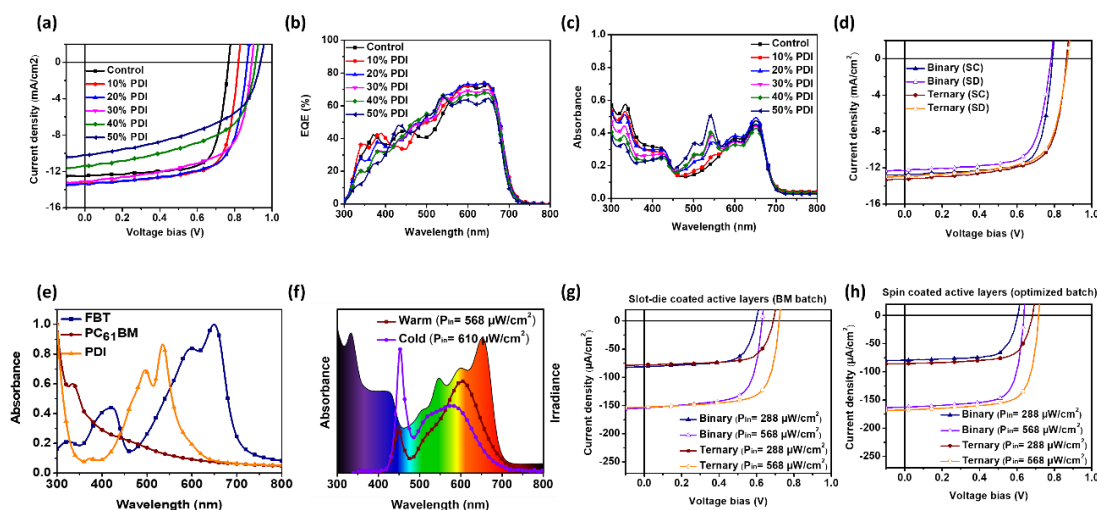


**Figure 13.** (a) Device  $J$ - $V$  curves of OPV devices with spin-coated active layers containing different PDI% in the ternary system under 1 sun illumination; (b,c) are the corresponding device EQE and UV-Vis optical absorption spectra, respectively. The control device corresponds to the binary FBT:PC<sub>61</sub>BM system, (d) device  $J$ - $V$  curves of OPV devices, spin-coated vs. slot-die, with binary and ternary active layers under 1 sun illumination, (e) optical absorption spectra of the neat films spin coated from *o*-xylene (10 mg/mL), (f) emission spectra of a 2700 K (warm) and 6500 K (cold) at 2000 lux LED illumination, with the optical absorption spectrum of the spin-coated ternary blend [FBT:PC<sub>61</sub>BM:PDI (1:1.2:0.3)] from a 20 mg/mL in *o*-xylene solution (containing 1% (*v/v*) p-anisaldehyde, AA) superimposed to show the match between the emission spectra of the LEDs and the absorption spectrum of the ternary blend, (g) device  $J$ - $V$  curves of OPV devices slot-die-coated with binary and ternary (20 wt.% PDI) active layers under different indoor light illuminations, and (h) device  $J$ - $V$  curves of OPV devices with spin-coated binary and ternary (20 wt.% PDI) active layers under different warm indoor light illuminations. ZnO/PEIE was used as the ETL [104]. (a–h) Reproduced with permission from [104]. Copyright 2020 American Chemical Society.

### Slot-Die-Coated Active Layers OPVs with High $V_{oc} > 1$ V

Our team further demonstrated the compound tPDI<sub>2</sub>N-EH as a versatile NFA by pairing it with different donor polymers, processing BHJs under a variety of conditions, and evaluating devices with a range of illumination intensities as detailed below. Achieving high  $V_{oc}$  values  $\geq 1$  V are desired for OPV devices; thus, quinoxaline-based donor polymers with deep HOMO energy levels are widely used to achieve such metrics. For our group, pairing such polymers with tPDI<sub>2</sub>N-EH allowed for the realization of high  $V_{oc}$  OPVs in which the BHJ was processed via slot-die-coating from halogen-free solvents [85,100,101].

Laventure et al. screened a series of BDT-QX donor polymers (QX1, QX2, QX3, QX4, Figure 5) with tPDI<sub>2</sub>N-EH and compared BHJ formation using spin coating and slot-die coating from non-halogenated solvents (Figure 14a–f) [100]. Spin-coated OPV devices with QX1, QX2, QX3, and QX4, blended with tPDI<sub>2</sub>N-EH provided PCEs of 5.7% ( $V_{oc} = 1.03$  V;  $J_{sc} = 9.4$  mA/cm<sup>2</sup>; FF = 59%), 4.8% ( $V_{oc} = 1.03$  V;  $J_{sc} = 8.5$  mA/cm<sup>2</sup>; FF = 54%), 4.5% ( $V_{oc} = 1.06$  V;  $J_{sc} = 7.6$  mA/cm<sup>2</sup>; FF = 55%), and 5.7% ( $V_{oc} = 1.04$  V;  $J_{sc} = 9.4$  mA/cm<sup>2</sup>; FF = 59%), respectively. Slot-die-coated devices based on the QX3 polymer resulted in a PCE of 4.1% ( $V_{oc} = 1.06$  V;  $J_{sc} = 7.0$  mA/cm<sup>2</sup>; FF = 56%). For all OPV devices, the  $V_{oc}$  was above 1 V. The diphenyl ether (DPE) solvent additive was found to be critical for increasing the device performance while maintaining a fully halogen-solvent-free processing.

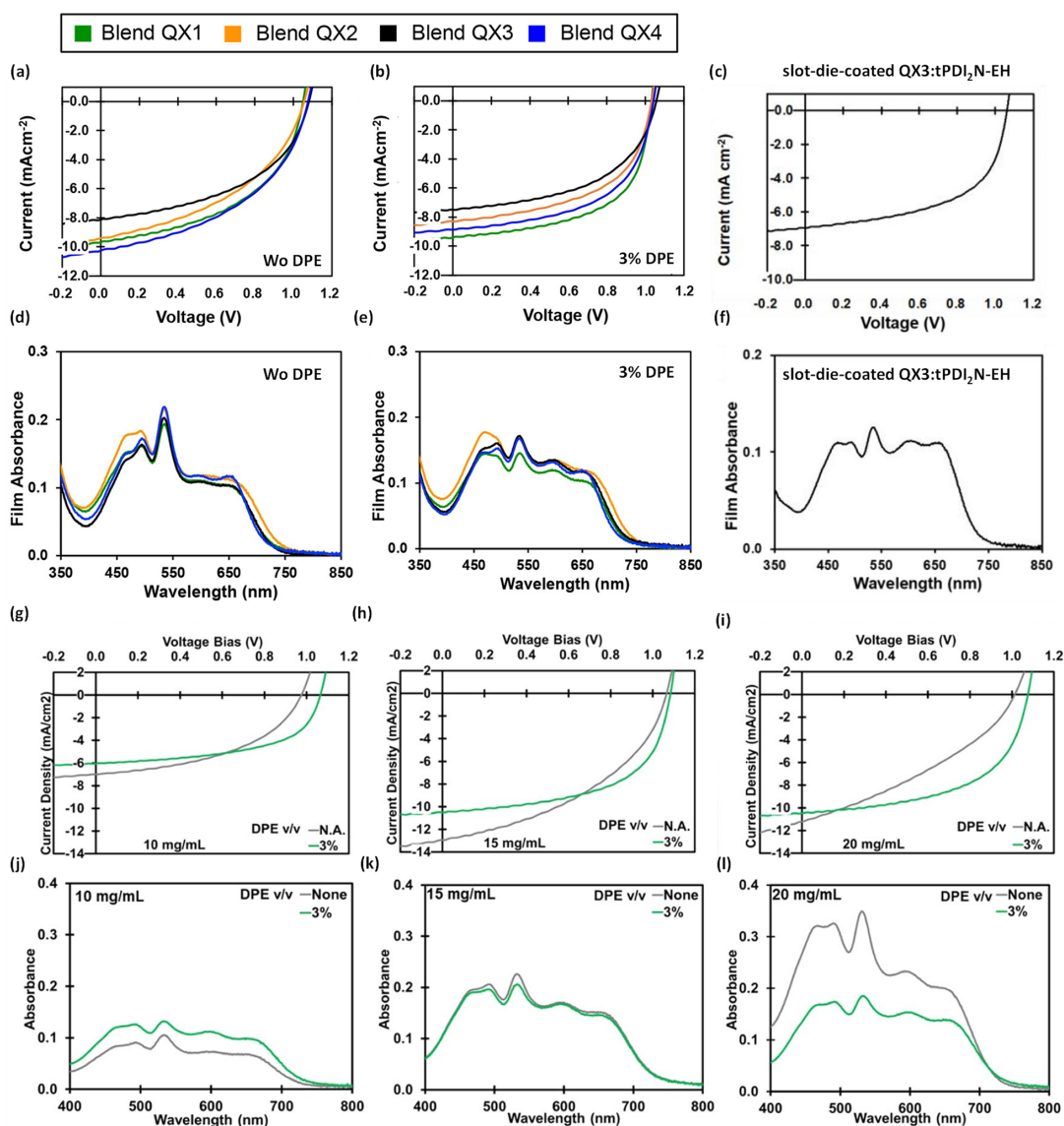


**Figure 14.** (a,b) Device  $J$ - $V$  curves of spin-coated OPVs using the QX1–QX4: tPDI<sub>2</sub>N-EH (1:1 blend) active layer processed from *o*-xylene without and with 3% DPE additive, (c) device  $J$ - $V$  curves of slot-die-coated OPVs using the QX3: tPDI<sub>2</sub>N-EH (1:1 blend) active layer processed from *o*-xylene without and with 3% DPE additive, (d–f) corresponding UV–Vis spectrum of the previous conditions, respectively, (g–i) device  $J$ - $V$  curves of slot-die-coated OPVs using the QX3: tPDI<sub>2</sub>N-EH (1:1 blend) active layer processed from toluene without and with 3% DPE additive at different total concentrations, (j–l) corresponding UV–Vis spectrum of the previous conditions, respectively. (a–f) and (g–l) reproduced with permissions from [100,101] respectively. Copyright 2019 American Chemical Society.

Follow-up work by Tontori et al. investigated the effect of solvent additives (DIO and DPE) on the blend morphology and aggregation behavior of BHJ blends based on QX3 and tPDI<sub>2</sub>N-EH [101]. Processing the BHJ with a DIO solvent additive induced excessive crystallization of tPDI<sub>2</sub>N-EH within the polymer matrix, leading to poor OPV performance, whereas processing the BHJ with DPE had a more suitable effect and, in turn, led to a boost in the OPV performance. OPV devices based on the QX3:tPDI<sub>2</sub>N-EH (1:1) BHJ with different solution concentrations (10, 15, and 20 mg/mL) were slot-die-coated from toluene with and without the DPE additive (Figure 14g–l) and compared to devices with spin-coated BHJs. OPV devices with BHJs processed with the DPE additive had a PCE of 7.3% ( $V_{oc} = 1.09$  V;  $J_{sc} = 12.4$  mA/cm<sup>2</sup>; FF = 54%) compared to a PCE of 6.6% ( $V_{oc} = 1.09$  V;  $J_{sc} = 11.7$  mA/cm<sup>2</sup>; FF = 51%) for those processed without the additive. A transition to slot-die-coated BHJs resulted in devices with a PCE of 6.5% ( $V_{oc} = 1.08$  V;  $J_{sc} = 10.5$  mA/cm<sup>2</sup>; FF = 58%) compared to a PCE of 6% ( $V_{oc} = 1.06$  V;  $J_{sc} = 13.0$  mA/cm<sup>2</sup>; FF = 43%) for devices processed without the additive. Little change was observed in the in device PCEs when transitioning from spin- to slot-die-coating methods (using halogen-free solvents in air) and, in all cases, the  $V_{oc}$  values were maintained above 1 V.

Further, the QX3 donor polymer was replaced with a simplified version, namely, PTQ10 polymer, which has a larger band gap ( $E_{gap}$ , ca 2.6 eV) and led to even higher  $V_{oc}$  values (Figure 5). OPV devices with a PTQ10:tPDI<sub>2</sub>N-EH BHJ processed using slot-die coating from halogen-free solvents had a PCE of 5% ( $V_{oc} = 1.2$  V;  $J_{sc} = 8.0$  mA/cm<sup>2</sup>; FF = 52%) under 1 sun illumination (AM1.5G; 100 mW/cm<sup>2</sup>). Similar OPV devices with spin-coated BHJs had a slightly higher PCE of 5.5% ( $V_{oc} = 1.21$  V;  $J_{sc} = 8.2$  mA/cm<sup>2</sup>; FF = 55%) (Figure 15c,d), again demonstrating that the tPDI<sub>2</sub>N-EH NFA can be easily transitioned to large-area devices. OPV devices were tested under low-light illumination conditions (ca. 400, 1000, and 2000 lux, both with 2700 K and 6500 K LED light, corresponding to  $P_{in}$  values between 113 and 610  $\mu$ W/cm<sup>2</sup>) and provided maximum PCEs of 10.1% ( $V_{oc} = 1.07$  V;  $J_{sc} = 105$   $\mu$ A/cm<sup>2</sup>; FF = 51%) and 10.4% ( $V_{oc} = 1.08$  V;  $J_{sc} = 118$   $\mu$ A/cm<sup>2</sup>; FF = 50%) with 2700 K and 6500 K, respectively (Figure 15f). These  $V_{oc}$  values are among the highest reported for indoor OPV devices [43]. To further improve the device PCEs, two strategies were examined: i) ZnO surface modification with PDICA (a carboxylic acid modified PDI), following a previous work reported by Abd-Ellah et al. [102], and ii) using the ternary approach by employing PDI-EDOT-PDI [115] as a third component in PTQ10:tPDI<sub>2</sub>N-EH. Using PDICA for ZnO modification enhanced PCEs under both 1 sun (PCE = 6.1%;  $V_{oc} = 1.24$  V;  $J_{sc} = 8.9$  mA/cm<sup>2</sup>; FF = 55%) and warm ca. 2000 lux LED illumination (PCE = 11.7%,  $V_{oc} = 1.07$  V;  $J_{sc} = 139$   $\mu$ A/cm<sup>2</sup>; FF = 48%), as shown in Figure 15g. With the ternary approach, a  $V_{oc}$  of 1.24 V under one sun illumination and 1.11 V under ca. 2000 lux LED illumination were achieved. Although the ternary approach resulted in reducing both the device  $J_{sc}$  and FF, leading to an overall lower PCE under 1 sun, a PCE of ~10% under ca. 2000 lux LED illumination (Figure 15h) was achieved.

### 3.4. Asymmetric Perylene Diimides NFAs

Asymmetric (or unsymmetrical) linear conjugated molecules have emerged as useful NFAs for high-performance OPV devices [116]. For example, asymmetric PDIs outperformed symmetric PDIs when used as NFAs in OPV devices (PCE = 6.6%;  $V_{oc} = 0.80$  V;  $J_{sc} = 14.8$  mA/cm<sup>2</sup>; FF = 56% vs. PCE = 4.5%;  $V_{oc} = 0.78$  V;  $J_{sc} = 14.4$  mA/cm<sup>2</sup>; FF = 40%) [117]. Our group reported on three different asymmetric PDIs and tested them as NFAs in OPV devices (Figure 16a) [82,106,107]. Payne et al. introduced the first asymmetric molecule (PDI-DPP-IQ) based on an NPDI, diketopyrrolopyrrole (DPP) and indoloquinoline (IQ) building units connected via C–C bonds in a linear fashion [82]. OPV devices based on PDI-DPP-IQ as an NFA, paired with P3HT as the donor polymer, showed a significant performance enhancement after chloroform SVA treatment, demonstrating a PCE of 0.8% ( $V_{oc} = 0.75$  V;  $J_{sc} = 2.5$  mA/cm<sup>2</sup>; FF = 42%) compared to a PCE of 0.1% ( $V_{oc} = 0.76$  V;  $J_{sc} = 0.6$  mA/cm<sup>2</sup>; FF = 26%) prior to SVA treatment (Figure 16b). The device performance enhancement was mainly attributed to a  $J_{sc}$  enhancement. The SVA treatment crystallized

the PDI-DPP-IQ, leading to a red-shifting of the absorption spectrum (Figure 16c). The enhancement in FF values after SVA treatment can be explained by the emergence of preferred structural rearrangement, forming well-defined nanomorphologies that enhanced charge extraction [82]. Despite the low PCE values, the new asymmetric chemical design is a guide for the development of future organic materials for organic electronics, especially in terms of bandgap engineering.

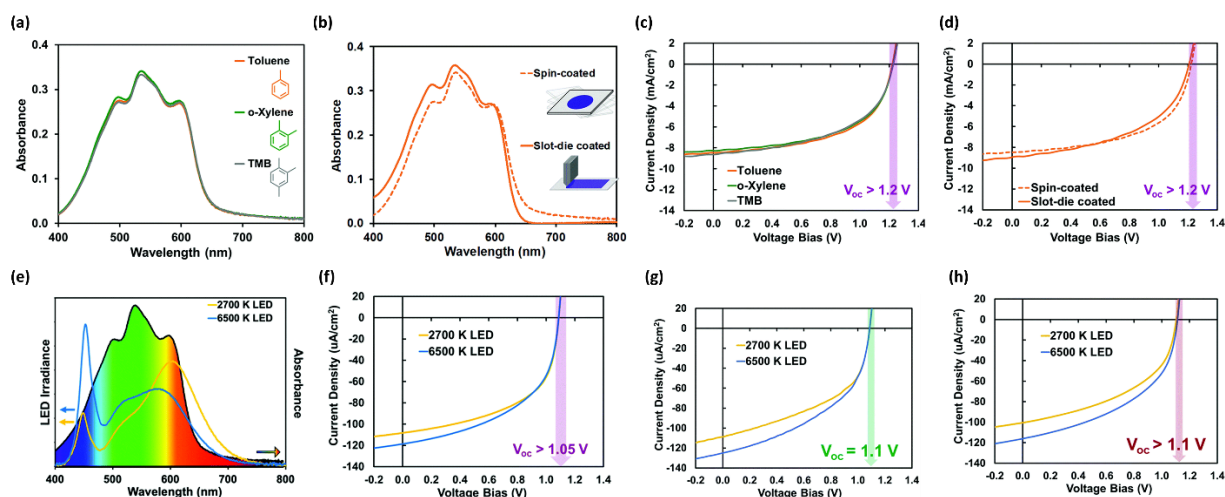


**Figure 15.** (a) UV-Vis absorption spectra of PTQ10:tPDI<sub>2</sub>N-EH (1:1) blend film from a toluene, *o*-xylene, or TMB solvent containing 1% (*v/v*) DPE, (b) UV-Vis absorption spectra of spin-coated and slot-die-coated films of the PTQ10:tPDI<sub>2</sub>N-EH (1:1) blend film from a 10 mg/mL and 15 mg/mL toluene solution, respectively, containing 1% (*v/v*) DPE, (c,d) the corresponding device *J*-*V* curves, respectively, under 1 sun illumination, (e) irradiance spectra of 2700 K and 6500 K LED, acting as the illumination source for the low-light intensity iOPV measurements. The optical absorption spectrum of the slot-die-coated blended film of the PTQ10:tPDI<sub>2</sub>N-EH (1:1) from a 15 mg/mL toluene solution containing 1% (*v/v*) DPE is superimposed to show the match between the emission spectrum of the LED and the absorption spectra of the blend, (f) device *J*-*V* curves of the corresponding OPVs tested under LED illumination of ca. 2000 lux (568 and 610  $\mu\text{W}/\text{cm}^2$  for 2700 K and 6500 K, respectively), and (g) device *J*-*V* curves of OPVs with PTQ10:tPDI<sub>2</sub>N-EH BHJs coated on top of ITO/ZnO/PDICA, and (h) device *J*-*V* curves of the ternary OPVs with PTQ10:tPDI<sub>2</sub>N-EH:PDI-EDOT-PDI (1:0.8:0.2) BHJs under 2000 lux LED illumination [85]. (a–h) reproduced with permission from [85]. Copyright 2020 Royal Society of Chemistry.

Next, the IQ dye was replaced with the N-(alkyl)benzothioxanthene-3,4-dicarboximide (BTXI) dye, delivering the molecule PDI-DPP-BTXI. This molecule exhibited ambipolar charge transport characteristics [106]. When paired with a PTB7-Th donor polymer, the OPV device performance was a modest 0.6% ( $V_{oc} = 1.0$  V;  $J_{sc} = 2.1$   $\text{mA}/\text{cm}^2$ ; FF = 27%). However, upon SVA treatment of the BHJ, the PCE doubled to 1.1% ( $V_{oc} = 0.95$  V;  $J_{sc} = 3.8$   $\text{mA}/\text{cm}^2$ ; FF = 31%), as shown in (Figure 14d,e). Next, the BTXI dye was replaced with a Se-annulated PDI dye (SePDI), producing the molecule NPDI-DPP-SePDI [107]. SVA treatment of the BHJ lead to a slight redshift accompanied by the emergence of a new high energy peak at 568 nm in the optical absorption spectrum. OPV devices with a BHJ comprising a PTB7-Th:NPDI-DPP-SePDI blend showed a slightly enhanced performance PCE of 0.8% ( $V_{oc} = 0.76$  V;  $J_{sc} = 2.7$   $\text{mA}/\text{cm}^2$ ; FF = 38%) with the BHJ SVA treatment compared to a PCE of 0.5% ( $V_{oc} = 0.76$  V;  $J_{sc} = 2.0$   $\text{mA}/\text{cm}^2$ ; FF = 37%) without the BHJ SVA treatment (Figure 16f,g). While the PCEs were low overall, the asymmetric-type PDIs offer unique optical profiles, energy cascades, and films susceptible to crystallization upon SVA treatment; therefore, further work is warranted to create structure–property–function relationships and develop higher-performing photoactive materials.

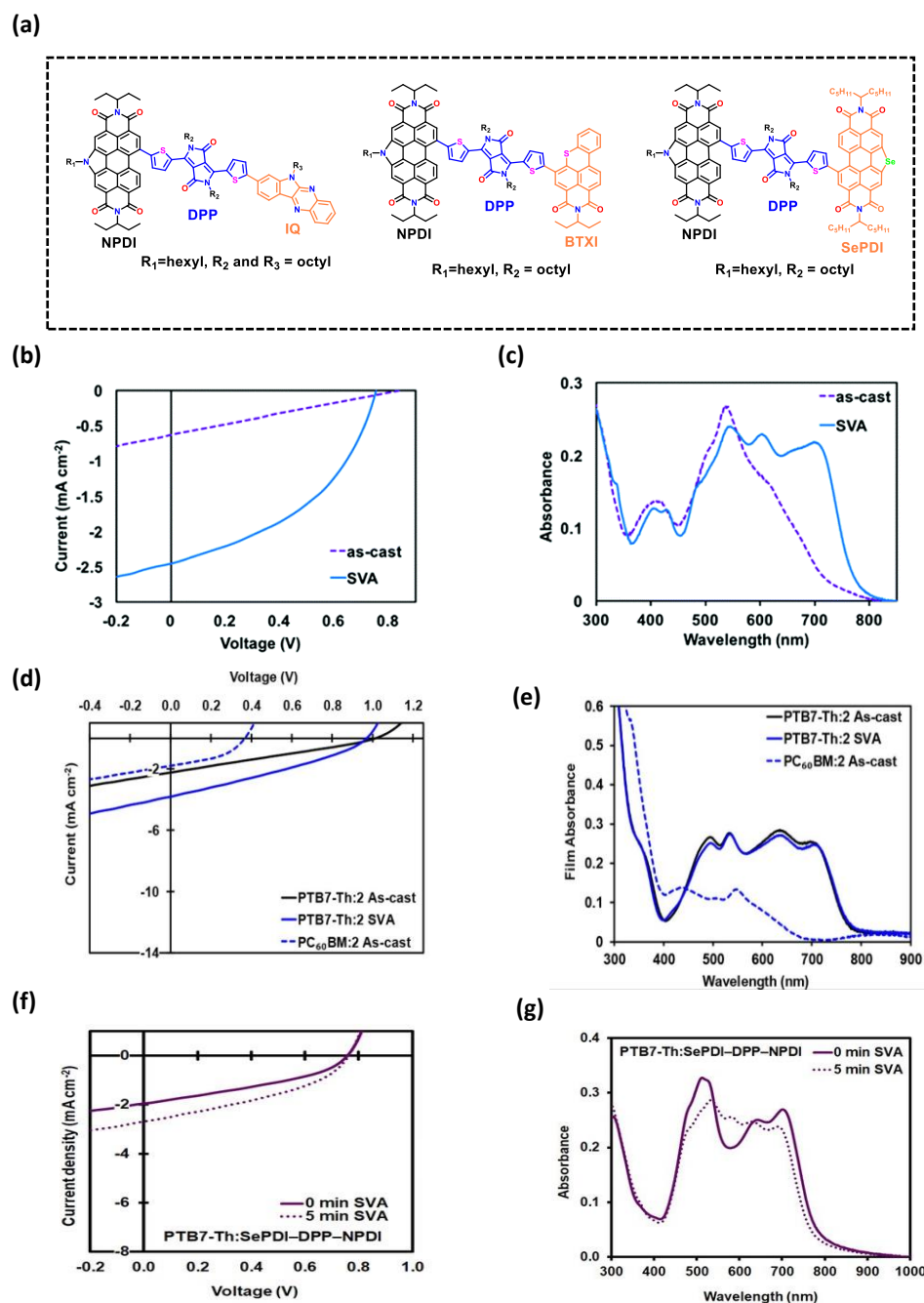


**Figure 16.** (a) Chemical structures of asymmetric PDI derivatives, (b) device *J-V* curves, and (c) UV-Vis absorption spectra of OPV devices based on a blend of P3HT:PDI-DPP-IQ [82]. (d) Device *J-V* curves (e) and UV-Vis absorption spectra of OPV devices based on a blend of PTB7-Th:PDI-DPP-BTXI [106]. (f) Device *J-V* curves and (g) UV-Vis absorption spectra of OPV devices based on a blend of PTB7-Th:NPDI-DPP-SePDI [107]. (b,c), (d,e), and (f,g) reproduced with permissions from [82,106,107], respectively. Copyright 2017 Royal Society of Chemistry, 2018 American Chemical Society and 2020 Wiley.

#### 4. Conclusions and Future Outlook

The N-annulated perylene diimide dye has proven to be a useful building block from which to construct molecular-based non-fullerene acceptors for use in organic photovoltaic cells. Key attributes of the N-annulation (in reference to the non-annulated perylene diimide) are: (1) a destabilization of the frontier molecular orbital energy levels, leading to a higher lying LUMO energy level which, in turn, allows for the realization of high open-circuit voltages in devices that are routinely over 1 V with a maximum-to-date of 1.2 V, and (2) an additional site for side-chain installation which renders the molecular compounds highly soluble in a range of suitable processing solvents, notably, halogen-free solvents (e.g., *o*-xylenes) and biocompatible solvents (e.g., 2-methyl THF), which has enabled the formation of large-area active layers via roll-to-roll compatible coating methods (e.g., slot-die coating). Owing to strong visible light optical absorption (characteristic of the perylene diimide chromophore), high device operating voltages, and an ability to be easily processed via slot-die coating, organic photovoltaic devices based on N-annulated perylene diimide non-fullerene acceptors have found best use in low-light applications, i.e., indoor photovoltaics. A key remaining challenge is boosting the lower-than-expected fill factor for the devices. A low electron mobility plagues these N-annulated perylene diimides, and strategies to tune the electronics and control the molecular self-assembly to enable highly ordered acceptor domains are warranted. The use of these compounds as third components in ternary blend active layers to enhance visible light absorption and boost voltages appears to be a promising route towards high-performance, roll-to-roll-processed organic photovoltaic devices. As a final comment, we would like to note is that beyond non-fullerene acceptor development, the N-annulated perylene diimide has proved quite useful for creating new electron transport layers for use in photovoltaic devices, offering an exciting opportunity for new molecular designs and synthetic strategies [118–123].

**Author Contributions:** Conceptualization, G.C.W.; writing—original draft preparation, M.E.F.; writing—review and editing, G.C.W.; supervision, G.C.W.; funding acquisition, G.C.W. All authors have read and agreed to the published version of the manuscript.

**Funding:** This work was funded by the NSERC DG program (2019-04392), the University of Calgary, and the Canada First Research Excellence Fund (CFREF).

**Acknowledgments:** Rahim Munir is thanked for initial work on this project gathering references and figure arrangement.

**Conflicts of Interest:** The authors declare no conflict of interest.

#### References

1. Kaltensbrunner, M.; White, M.S.; Głowacki, E.D.; Sekitani, T.; Someya, T.; Sariciftci, N.S.; Bauer, S. Ultrathin and Lightweight Organic Solar Cells with High Flexibility. *Nat. Commun.* **2012**, *3*, 770. [[CrossRef](#)] [[PubMed](#)]
2. Fukuda, K.; Yu, K.; Someya, T. The Future of Flexible Organic Solar Cells. *Adv. Energy Mater.* **2020**, *10*, 2000765. [[CrossRef](#)]
3. Søndergaard, R.; Hösel, M.; Angmo, D.; Larsen-Olsen, T.T.; Krebs, F.C. Roll-to-Roll Fabrication of Polymer Solar Cells. *Mater. Today* **2012**, *15*, 36–49. [[CrossRef](#)]
4. Krebs, F.C. Fabrication and Processing of Polymer Solar Cells: A Review of Printing and Coating Techniques. *Sol. Energy Mater. Sol. Cells* **2009**, *93*, 394–412. [[CrossRef](#)]
5. Kim, Y.; Son, J.; Shafian, S.; Kim, K.; Hyun, J.K. Semitransparent Blue, Green, and Red Organic Solar Cells Using Color Filtering Electrodes. *Adv. Opt. Mater.* **2018**, *6*, 1800051. [[CrossRef](#)]
6. Li, Y.; Guo, X.; Peng, Z.; Qu, B.; Yan, H.; Ade, H.; Zhang, M.; Forrest, S.R. Color-Neutral, Semitransparent Organic Photovoltaics for Power Window Applications. *Proc. Natl. Acad. Sci. USA* **2020**, *117*, 21147–21154. [[CrossRef](#)]
7. Li, Z.; Ma, T.; Yang, H.; Lu, L.; Wang, R. Transparent and Colored Solar Photovoltaics for Building Integration. *Sol. RRL* **2020**, *5*, 2000614. [[CrossRef](#)]
8. Yang, C.; Sheng, W.; Moemeni, M.; Bates, M.; Herrera, C.K.; Borhan, B.; Lunt, R.R. Ultraviolet and Near-Infrared Dual-Band Selective-Harvesting Transparent Luminescent Solar Concentrators. *Adv. Energy Mater.* **2021**, *11*, 2003581. [[CrossRef](#)]
9. Jinno, H.; Fukuda, K.; Xu, X.; Park, S.; Suzuki, Y.; Koizumi, M.; Yokota, T.; Osaka, I.; Takimiya, K.; Someya, T. Stretchable and Waterproof Elastomer-Coated Organic Photovoltaics for Washable Electronic Textile Applications. *Nat. Energy* **2017**, *2*, 780–785. [[CrossRef](#)]
10. Tang, C.W. Two-layer Organic Photovoltaic Cell. *Appl. Phys. Lett.* **1986**, *48*, 183–185. [[CrossRef](#)]

11. Spanggaard, H.; Krebs, F.C. A Brief History of the Development of Organic and Polymeric Photovoltaics. *Sol. Energy Mater. Sol. Cells* **2004**, *83*, 125–146. [[CrossRef](#)]
12. Yu, G.; Gao, J.; Hummelen, J.C.; Wudl, F.; Heeger, A.J. Polymer Photovoltaic Cells: Enhanced Efficiencies via a Network of Internal Donor-Acceptor Heterojunctions. *Science* **1995**, *270*, 1789–1791. [[CrossRef](#)]
13. Chen, J.; Cao, Y. Development of Novel Conjugated Donor Polymers for High-Efficiency Bulk-Heterojunction Photovoltaic Devices. *Acc. Chem. Res.* **2009**, *42*, 1709–1718. [[CrossRef](#)] [[PubMed](#)]
14. Roncali, J. Molecular Bulk Heterojunctions: An Emerging Approach to Organic Solar Cells. *Acc. Chem. Res.* **2009**, *42*, 1719–1730. [[CrossRef](#)]
15. Cheng, Y.-J.; Yang, S.-H.; Hsu, C.-S. Synthesis of Conjugated Polymers for Organic Solar Cell Applications. *Chem. Rev.* **2009**, *109*, 5868–5923. [[CrossRef](#)]
16. Lai, Y.-Y.; Cheng, Y.-J.; Hsu, C.-S. Applications of Functional Fullerene Materials in Polymer Solar Cells. *Energy Environ. Sci.* **2014**, *7*, 1866–1883. [[CrossRef](#)]
17. Li, Y. Fullerene-Bisadduct Acceptors for Polymer Solar Cells. *Chem.-Asian J.* **2013**, *8*, 2316–2328. [[CrossRef](#)]
18. He, Y.; Li, Y. Fullerene Derivative Acceptors for High Performance Polymer Solar Cells. *Phys. Chem. Chem. Phys.* **2011**, *13*, 1970–1983. [[CrossRef](#)]
19. Peet, J.; Heeger, A.J.; Bazan, G.C. “Plastic” Solar Cells: Self-Assembly of Bulk Heterojunction Nanomaterials by Spontaneous Phase Separation. *Acc. Chem. Res.* **2009**, *42*, 1700–1708. [[CrossRef](#)]
20. Würthner, F.; Meerholz, K. Systems Chemistry Approach in Organic Photovoltaics. *Chem.-Eur. J.* **2010**, *16*, 9366–9373. [[CrossRef](#)]
21. Heeger, A.J. 25th Anniversary Article: Bulk Heterojunction Solar Cells: Understanding the Mechanism of Operation. *Adv. Mater.* **2014**, *26*, 10–28. [[CrossRef](#)] [[PubMed](#)]
22. Dou, L.; You, J.; Hong, Z.; Xu, Z.; Li, G.; Street, R.A.; Yang, Y. 25th Anniversary Article: A Decade of Organic/Polymeric Photovoltaic Research. *Adv. Mater.* **2013**, *25*, 6642–6671. [[CrossRef](#)]
23. Blom, P.W.M.; Mihailetschi, V.D.; Koster, L.J.A.; Markov, D.E. Device Physics of Polymer:Fullerene Bulk Heterojunction Solar Cells. *Adv. Mater.* **2007**, *19*, 1551–1566. [[CrossRef](#)]
24. Lee, C.-K.; Pao, C.-W.; Chu, C.-W. Multiscale Molecular Simulations of the Nanoscale Morphologies of P3HT:PCBM Blends for Bulk Heterojunction Organic Photovoltaic Cells. *Energy Environ. Sci.* **2011**, *4*, 4124–4132. [[CrossRef](#)]
25. Hummelen, J.C.; Knight, B.W.; LePeq, F.; Wudl, F.; Yao, J.; Wilkins, C.L. Preparation and Characterization of Fulleroid and Methanofullerene Derivatives. *J. Org. Chem.* **1995**, *60*, 532–538. [[CrossRef](#)]
26. Wienk, M.M.; Kroon, J.M.; Verhees, W.J.H.; Knol, J.; Hummelen, J.C.; van Hal, P.A.; Janssen, R.A.J. Efficient Methano[70]Fullerene/MDMO-PPV Bulk Heterojunction Photovoltaic Cells. *Angew. Chem. Int. Ed.* **2003**, *42*, 3371–3375. [[CrossRef](#)] [[PubMed](#)]
27. Liu, T.; Troisi, A. What Makes Fullerene Acceptors Special as Electron Acceptors in Organic Solar Cells and How to Replace Them. *Adv. Mater.* **2013**, *25*, 1038–1041. [[CrossRef](#)]
28. Liu, Y.; Zhao, J.; Li, Z.; Mu, C.; Ma, W.; Hu, H.; Jiang, K.; Lin, H.; Ade, H.; Yan, H. Aggregation and Morphology Control Enables Multiple Cases of High-Efficiency Polymer Solar Cells. *Nat. Commun.* **2014**, *5*, 5293. [[CrossRef](#)]
29. He, Z.; Xiao, B.; Liu, F.; Wu, H.; Yang, Y.; Xiao, S.; Wang, C.; Russell, T.P.; Cao, Y. Single-Junction Polymer Solar Cells with High Efficiency and Photovoltage. *Nat. Photonics* **2015**, *9*, 174–179. [[CrossRef](#)]
30. Zhao, J.; Li, Y.; Yang, G.; Jiang, K.; Lin, H.; Ade, H.; Ma, W.; Yan, H. Efficient Organic Solar Cells Processed from Hydrocarbon Solvents. *Nat. Energy* **2016**, *1*, 1–7. [[CrossRef](#)]
31. Meredith, P.; Li, W.; Armin, A. Nonfullerene Acceptors: A Renaissance in Organic Photovoltaics? *Adv. Energy Mater.* **2020**, *10*, 2001788. [[CrossRef](#)]
32. Hou, J.; Inganäs, O.; Friend, R.H.; Gao, F. Organic Solar Cells Based on Non-Fullerene Acceptors. *Nat. Mater.* **2018**, *17*, 119–128. [[CrossRef](#)]
33. Liu, Q.; Jiang, Y.; Jin, K.; Qin, J.; Xu, J.; Li, W.; Xiong, J.; Liu, J.; Xiao, Z.; Sun, K.; et al. 18% Efficiency Organic Solar Cells. *Sci. Bull.* **2020**, *65*, 272–275. [[CrossRef](#)]
34. Zhang, M.; Zhu, L.; Zhou, G.; Hao, T.; Qiu, C.; Zhao, Z.; Hu, Q.; Larson, B.W.; Zhu, H.; Ma, Z.; et al. Single-Layered Organic Photovoltaics with Double Cascading Charge Transport Pathways: 18% Efficiencies. *Nat. Commun.* **2021**, *12*, 309. [[CrossRef](#)] [[PubMed](#)]
35. Lin, Y.; Nugraha, M.I.; Firdaus, Y.; Scaccabarozzi, A.D.; Anié, F.; Emwas, A.-H.; Yengel, E.; Zheng, X.; Liu, J.; Wahyudi, W.; et al. A Simple N-Dopant Derived from Diquat Boosts the Efficiency of Organic Solar Cells to 18.3%. *ACS Energy Lett.* **2020**, *5*, 3663–3671. [[CrossRef](#)]
36. Firdaus, Y.; Corre, V.M.L.; Khan, J.I.; Kan, Z.; Laquai, F.; Beaujuge, P.M.; Anthopoulos, T.D. Key Parameters Requirements for Non-Fullerene-Based Organic Solar Cells with Power Conversion Efficiency >20%. *Adv. Sci.* **2019**, *6*, 1802028. [[CrossRef](#)] [[PubMed](#)]
37. Li, N.; McCulloch, I.; Brabec, C.J. Analyzing the Efficiency, Stability and Cost Potential for Fullerene-Free Organic Photovoltaics in One Figure of Merit. *Energy Environ. Sci.* **2018**, *11*, 1355–1361. [[CrossRef](#)]
38. Li, N.; Brabec, C.J. Washing Away Barriers. *Nat. Energy* **2017**, *2*, 772–773. [[CrossRef](#)]
39. Lee, B.; Lahann, L.; Li, Y.; Forrest, S.R. Cost Estimates of Production Scale Semitransparent Organic Photovoltaic Modules for Building Integrated Photovoltaics. *Sustain. Energy Fuels* **2020**, *4*, 5765–5772. [[CrossRef](#)]

40. Han, C.; Wang, J.; Zhang, S.; Chen, L.; Bi, F.; Wang, J.; Yang, C.; Wang, P.; Li, Y.; Bao, X. Over 19% Efficiency Organic Solar Cells by Regulating Multidimensional Intermolecular Interactions. *Adv. Mater.* **2023**, *35*, 2208986. [[CrossRef](#)] [[PubMed](#)]
41. Liao, C.-Y.; Hsiao, Y.-T.; Tsai, K.-W.; Teng, N.-W.; Li, W.-L.; Wu, J.-L.; Kao, J.-C.; Lee, C.-C.; Yang, C.-M.; Tan, H.-S.; et al. Photoactive Material for Highly Efficient and All Solution-Processed Organic Photovoltaic Modules: Study on the Efficiency, Stability, and Synthetic Complexity. *Sol. RRL* **2021**, *5*, 2000749. [[CrossRef](#)]
42. Ylikunnari, M.; Välimäki, M.; Väisänen, K.-L.; Kraft, T.M.; Sliz, R.; Corso, G.; Po, R.; Barbieri, R.; Carbonera, C.; Gorni, G.; et al. Flexible OPV Modules for Highly Efficient Indoor Applications. *Flex. Print. Electron.* **2020**, *5*, 014008. [[CrossRef](#)]
43. Cui, Y.; Wang, Y.; Bergqvist, J.; Yao, H.; Xu, Y.; Gao, B.; Yang, C.; Zhang, S.; Inganäs, O.; Gao, F.; et al. Wide-Gap Non-Fullerene Acceptor Enabling High-Performance Organic Photovoltaic Cells for Indoor Applications. *Nat. Energy* **2019**, *4*, 768–775. [[CrossRef](#)]
44. Steim, R.; Ameri, T.; Schilinsky, P.; Waldauf, C.; Dennler, G.; Scharber, M.; Brabec, C.J. Organic Photovoltaics for Low Light Applications. *Sol. Energy Mater. Sol. Cells* **2011**, *95*, 3256–3261. [[CrossRef](#)]
45. Cutting, C.L.; Bag, M.; Venkataraman, D. Indoor Light Recycling: A New Home for Organic Photovoltaics. *J. Mater. Chem. C* **2016**, *4*, 10367–10370. [[CrossRef](#)]
46. Mainville, M.; Leclerc, M. Recent Progress on Indoor Organic Photovoltaics: From Molecular Design to Production Scale. *ACS Energy Lett.* **2020**, *5*, 1186–1197. [[CrossRef](#)]
47. Ryu, H.S.; Park, S.Y.; Lee, T.H.; Kim, J.Y.; Woo, H.Y. Recent Progress in Indoor Organic Photovoltaics. *Nanoscale* **2020**, *12*, 5792–5804. [[CrossRef](#)] [[PubMed](#)]
48. Yan, N.; Zhao, C.; You, S.; Zhang, Y.; Li, W. Recent Progress of Thin-Film Photovoltaics for Indoor Application. *Chin. Chem. Lett.* **2020**, *31*, 643–653. [[CrossRef](#)]
49. Kippelen, B.; Brédas, J.-L. Organic Photovoltaics. *Energy Environ. Sci.* **2009**, *2*, 251–261. [[CrossRef](#)]
50. Su, Y.-W.; Lan, S.-C.; Wei, K.-H. Organic Photovoltaics. *Mater. Today* **2012**, *15*, 554–562. [[CrossRef](#)]
51. Mazzio, K.A.; Luscombe, C.K. The Future of Organic Photovoltaics. *Chem. Soc. Rev.* **2014**, *44*, 78–90. [[CrossRef](#)]
52. Lipomi, D.J. Organic Photovoltaics: Focus on Its Strengths. *Joule* **2018**, *2*, 195–198. [[CrossRef](#)]
53. Zhao, F.; Wang, C.; Zhan, X. Morphology Control in Organic Solar Cells. *Adv. Energy Mater.* **2018**, *8*, 1703147. [[CrossRef](#)]
54. Zhang, G.; Zhao, J.; Chow, P.C.Y.; Jiang, K.; Zhang, J.; Zhu, Z.; Zhang, J.; Huang, F.; Yan, H. Nonfullerene Acceptor Molecules for Bulk Heterojunction Organic Solar Cells. *Chem. Rev.* **2018**, *118*, 3447–3507. [[CrossRef](#)] [[PubMed](#)]
55. Sonar, P.; Lim, J.P.F.; Chan, K.L. Organic Non-Fullerene Acceptors for Organic Photovoltaics. *Energy Environ. Sci.* **2011**, *4*, 1558–1574. [[CrossRef](#)]
56. Lin, Y.; Wang, J.; Zhang, Z.-G.; Bai, H.; Li, Y.; Zhu, D.; Zhan, X. An Electron Acceptor Challenging Fullerenes for Efficient Polymer Solar Cells. *Adv. Mater.* **2015**, *27*, 1170–1174. [[CrossRef](#)]
57. Zhao, W.; Li, S.; Yao, H.; Zhang, S.; Zhang, Y.; Yang, B.; Hou, J. Molecular Optimization Enables over 13% Efficiency in Organic Solar Cells. *J. Am. Chem. Soc.* **2017**, *139*, 7148–7151. [[CrossRef](#)]
58. Zhu, L.; Zhang, M.; Xu, J.; Li, C.; Yan, J.; Zhou, G.; Zhong, W.; Hao, T.; Song, J.; Xue, X.; et al. Single-Junction Organic Solar Cells with over 19% Efficiency Enabled by a Refined Double-Fibril Network Morphology. *Nat. Mater.* **2022**, *21*, 656–663. [[CrossRef](#)]
59. Yang, Y. The Original Design Principles of the Y-Series Nonfullerene Acceptors, from Y1 to Y6. *ACS Nano* **2021**, *15*, 18679–18682. [[CrossRef](#)]
60. Liu, S.; Yuan, J.; Deng, W.; Luo, M.; Xie, Y.; Liang, Q.; Zou, Y.; He, Z.; Wu, H.; Cao, Y. High-Efficiency Organic Solar Cells with Low Non-Radiative Recombination Loss and Low Energetic Disorder. *Nat. Photonics* **2020**, *14*, 300–305. [[CrossRef](#)]
61. Liu, J.; Chen, S.; Qian, D.; Gautam, B.; Yang, G.; Zhao, J.; Bergqvist, J.; Zhang, F.; Ma, W.; Ade, H.; et al. Fast Charge Separation in a Non-Fullerene Organic Solar Cell with a Small Driving Force. *Nat. Energy* **2016**, *1*, 16089. [[CrossRef](#)]
62. Ding, K.; Shan, T.; Xu, J.; Li, M.; Wang, Y.; Zhang, Y.; Xie, Z.; Ma, Z.; Liu, F.; Zhong, H. A Perylene Diimide-Containing Acceptor Enables High Fill Factor in Organic Solar Cells. *Chem. Commun.* **2020**, *56*, 11433–11436. [[CrossRef](#)]
63. Kozma, E.; Catellani, M. Perylene Diimides Based Materials for Organic Solar Cells. *Dyes Pigments* **2013**, *98*, 160–179. [[CrossRef](#)]
64. Liu, Z.; Wu, Y.; Zhang, Q.; Gao, X. Non-Fullerene Small Molecule Acceptors Based on Perylene Diimides. *J. Mater. Chem. A* **2016**, *4*, 17604–17622. [[CrossRef](#)]
65. Macedo, A.G.; Christopholi, L.P.; Gavim, A.E.X.; de Deus, J.F.; Teridi, M.A.M.; Yusoff, A.R.b.M.; da Silva, W.J. Perylene Derivatives for Solar Cells and Energy Harvesting: A Review of Materials, Challenges and Advances. *J. Mater. Sci. Mater. Electron.* **2019**, *30*, 15803–15824. [[CrossRef](#)]
66. Nowak-Król, A.; Shoyama, K.; Stolte, M.; Würthner, F. Naphthalene and Perylene Diimides—Better Alternatives to Fullerenes for Organic Electronics? *Chem. Commun.* **2018**, *54*, 13763–13772. [[CrossRef](#)] [[PubMed](#)]
67. Zink-Lorre, N.; Font-Sanchis, E.; Sastre-Santos, Á.; Fernández-Lázaro, F. Perylenediimides as More than Just Non-Fullerene Acceptors: Versatile Components in Organic, Hybrid and Perovskite Solar Cells. *Chem. Commun.* **2020**, *56*, 3824–3838. [[CrossRef](#)]
68. Fujimoto, K.; Takahashi, M.; Izawa, S.; Hiramoto, M. Development of Perylene-Based Non-Fullerene Acceptors through Bay-Functionalization Strategy. *Materials* **2020**, *13*, 2148. [[CrossRef](#)] [[PubMed](#)]
69. Duan, Y.; Xu, X.; Li, Y.; Peng, Q. Recent Development of Perylene Diimide-Based Small Molecular Non-Fullerene Acceptors in Organic Solar Cells. *Chin. Chem. Lett.* **2017**, *28*, 2105–2115. [[CrossRef](#)]
70. He, Q.; Kafourou, P.; Hu, X.; Heeney, M. Development of Non-Fullerene Electron Acceptors for Efficient Organic Photovoltaics. *SN Appl. Sci.* **2022**, *4*, 247. [[CrossRef](#)]

71. Liu, T.; Guo, Y.; Yi, Y.; Huo, L.; Xue, X.; Sun, X.; Fu, H.; Xiong, W.; Meng, D.; Wang, Z.; et al. Ternary Organic Solar Cells Based on Two Compatible Nonfullerene Acceptors with Power Conversion Efficiency >10%. *Adv. Mater.* **2016**, *28*, 10008–10015. [[CrossRef](#)] [[PubMed](#)]
72. Zhang, J.; Li, Y.; Huang, J.; Hu, H.; Zhang, G.; Ma, T.; Chow, P.C.Y.; Ade, H.; Pan, D.; Yan, H. Ring-Fusion of Perylene Diimide Acceptor Enabling Efficient Nonfullerene Organic Solar Cells with a Small Voltage Loss. *J. Am. Chem. Soc.* **2017**, *139*, 16092–16095. [[CrossRef](#)] [[PubMed](#)]
73. Ma, L.-K.; Chen, Y.; Chow, P.C.Y.; Zhang, G.; Huang, J.; Ma, C.; Zhang, J.; Yin, H.; Hong Cheung, A.M.; Wong, K.S.; et al. High-Efficiency Indoor Organic Photovoltaics with a Band-Aligned Interlayer. *Joule* **2020**, *4*, 1486–1500. [[CrossRef](#)]
74. Sharenko, A.; Proctor, C.M.; Poll, T.S.v.d.; Henson, Z.B.; Nguyen, T.-Q.; Bazan, G.C. A High-Performing Solution-Processed Small Molecule: Perylene Diimide Bulk Heterojunction Solar Cell. *Adv. Mater.* **2013**, *25*, 4403–4406. [[CrossRef](#)]
75. Schmidt-Mende, L. Self-Organized Discotic Liquid Crystals for High-Efficiency Organic Photovoltaics. *Science* **2001**, *293*, 1119–1122. [[CrossRef](#)]
76. Meng, D.; Sun, D.; Zhong, C.; Liu, T.; Fan, B.; Huo, L.; Li, Y.; Jiang, W.; Choi, H.; Kim, T.; et al. High-Performance Solution-Processed Non-Fullerene Organic Solar Cells Based on Selenophene-Containing Perylene Bisimide Acceptor. *J. Am. Chem. Soc.* **2016**, *138*, 375–380. [[CrossRef](#)] [[PubMed](#)]
77. Sun, D.; Meng, D.; Cai, Y.; Fan, B.; Li, Y.; Jiang, W.; Huo, L.; Sun, Y.; Wang, Z. Non-Fullerene-Acceptor-Based Bulk-Heterojunction Organic Solar Cells with Efficiency over 7%. *J. Am. Chem. Soc.* **2015**, *137*, 11156–11162. [[CrossRef](#)] [[PubMed](#)]
78. Duan, Y.; Xu, X.; Yan, H.; Wu, W.; Li, Z.; Peng, Q. Pronounced Effects of a Triazine Core on Photovoltaic Performance—Efficient Organic Solar Cells Enabled by a PDI Trimer-Based Small Molecular Acceptor. *Adv. Mater.* **2017**, *29*, 1605115. [[CrossRef](#)] [[PubMed](#)]
79. Jiang, W.; Ye, L.; Li, X.; Xiao, C.; Tan, F.; Zhao, W.; Hou, J.; Wang, Z. Bay-Linked Perylene Bisimides as Promising Non-Fullerene Acceptors for Organic Solar Cells. *Chem. Commun.* **2013**, *50*, 1024–1026. [[CrossRef](#)]
80. Langhals, H.; Kirner, S. Novel Fluorescent Dyes by the Extension of the Core of Perylenetetra-carboxylic Bisimides. *Eur. J. Org. Chem.* **2000**, *2000*, 365–380. [[CrossRef](#)]
81. Hendsbee, A.D.; Sun, J.-P.; Law, W.K.; Yan, H.; Hill, I.G.; Spasyuk, D.M.; Welch, G.C. Synthesis, Self-Assembly, and Solar Cell Performance of N-Annulated Perylene Diimide Non-Fullerene Acceptors. *Chem. Mater.* **2016**, *28*, 7098–7109. [[CrossRef](#)]
82. Payne, A.-J.; Li, S.; Dayneko, S.V.; Risko, C.; Welch, G.C. An Unsymmetrical Non-Fullerene Acceptor: Synthesis via Direct Heteroarylation, Self-Assembly, and Utility as a Low Energy Absorber in Organic Photovoltaic Cells. *Chem. Commun.* **2017**, *53*, 10168–10171. [[CrossRef](#)]
83. Dayneko, S.V.; Hendsbee, A.D.; Welch, G.C. Fullerene-Free Polymer Solar Cells Processed from Non-Halogenated Solvents in Air with PCE of 4.8%. *Chem. Commun.* **2017**, *53*, 1164–1167. [[CrossRef](#)] [[PubMed](#)]
84. McAfee, S.M.; Dayneko, S.V.; Josse, P.; Blanchard, P.; Cabanetos, C.; Welch, G.C. Simply Complex: The Efficient Synthesis of an Intricate Molecular Acceptor for High-Performance Air-Processed and Air-Tested Fullerene-Free Organic Solar Cells. *Chem. Mater.* **2017**, *29*, 1309–1314. [[CrossRef](#)]
85. Tintori, F.; Laventure, A.; Koenig, J.D.B.; Welch, G.C. High Open-Circuit Voltage Roll-to-Roll Compatible Processed Organic Photovoltaics. *J. Mater. Chem. C* **2020**, *8*, 13430–13438. [[CrossRef](#)]
86. McAfee, S.M.; Dayneko, S.V.; Hendsbee, A.D.; Josse, P.; Blanchard, P.; Cabanetos, C.; Welch, G.C. Applying Direct Heteroarylation Synthesis to Evaluate Organic Dyes as the Core Component in PDI-Based Molecular Materials for Fullerene-Free Organic Solar Cells. *J. Mater. Chem. A* **2017**, *5*, 11623–11633. [[CrossRef](#)]
87. McAfee, S.M.; Payne, A.-J.; Hendsbee, A.D.; Xu, S.; Zou, Y.; Welch, G.C. Toward a Universally Compatible Non-Fullerene Acceptor: Multi-Gram Synthesis, Solvent Vapor Annealing Optimization, and BDT-Based Polymer Screening. *Sol. RRL* **2018**, *2*, 1800143. [[CrossRef](#)]
88. Koenig, J.D.; Farahat, M.; Dhindsa, J.; Gilroy, J.; Welch, G. Near-IR Absorption and Photocurrent Generation Using a First-of-Its-Kind Boron Difluoride Formazanate Non-Fullerene Acceptor. *Mater. Chem. Front.* **2020**, *4*, 1643–1647. [[CrossRef](#)]
89. Hendsbee, A.D.; Dayneko, S.V.; Pells, J.A.; Cann, J.R.; Welch, G.C. N-Annulated Perylene Diimide Dimers: The Effect of Thiophene Bridges on Physical, Electronic, Optical, and Photovoltaic Properties. *Sustain. Energy Fuels* **2017**, *1*, 1137–1147. [[CrossRef](#)]
90. Laventure, A.; Stanzel, S.; Payne, A.-J.; Lessard, B.H.; Welch, G.C. A Ring Fused N-Annulated PDI Non-Fullerene Acceptor for High Open Circuit Voltage Solar Cells Processed from Non-Halogenated Solvents. *Synth. Met.* **2019**, *250*, 55–62. [[CrossRef](#)]
91. Welsh, T.A.; Laventure, A.; Baumgartner, T.; Welch, G.C. Dithienophosphole-Based Molecular Electron Acceptors Constructed Using Direct (Hetero)Arylation Cross-Coupling Methods. *J. Mater. Chem. C* **2018**, *6*, 2148–2154. [[CrossRef](#)]
92. Welsh, T.A.; Laventure, A.; Alahmadi, A.F.; Zhang, G.; Baumgartner, T.; Zou, Y.; Jäkle, F.; Welch, G.C. Borane Incorporation in a Non-Fullerene Acceptor To Tune Steric and Electronic Properties and Improve Organic Solar Cell Performance. *ACS Appl. Energy Mater.* **2019**, *2*, 1229–1240. [[CrossRef](#)]
93. Welsh, T.A.; Laventure, A.; Welch, G.C. Direct (Hetero)Arylation for the Synthesis of Molecular Materials: Coupling Thieno[3,4-c]Pyrrole-4,6-Dione with Perylene Diimide to Yield Novel Non-Fullerene Acceptors for Organic Solar Cells. *Molecules* **2018**, *23*, 931. [[CrossRef](#)] [[PubMed](#)]
94. Payne, A.-J.; Song, J.; Sun, Y.; Welch, G.C. A Tetrameric Perylene Diimide Non-Fullerene Acceptor via Unprecedented Direct (Hetero)Arylation Cross-Coupling Reactions. *Chem. Commun.* **2018**, *54*, 11443–11446. [[CrossRef](#)] [[PubMed](#)]
95. Koenig, J.D.B.; Laventure, A.; Welch, G.C. Harnessing Direct (Hetero)Arylation in Pursuit of a Saddle-Shaped Perylene Diimide Tetramer. *ACS Appl. Energy Mater.* **2019**, *2*, 8939–8945. [[CrossRef](#)]

96. Vespa, M.; Cann, J.R.; Dayneko, S.V.; Melville, O.A.; Hendsbee, A.D.; Zou, Y.; Lessard, B.H.; Welch, G.C. Synthesis of a Perylene Diimide Dimer with Pyrrolic N–H Bonds and N-Functionalized Derivatives for Organic Field-Effect Transistors and Organic Solar Cells. *Eur. J. Org. Chem.* **2018**, *2018*, 4592–4599. [[CrossRef](#)]
97. Cann, J.; Dayneko, S.; Sun, J.-P.; Hendsbee, A.D.; Hill, I.G.; Welch, G.C. N-Annulated Perylene Diimide Dimers: Acetylene Linkers as a Strategy for Controlling Structural Conformation and the Impact on Physical, Electronic, Optical and Photovoltaic Properties. *J. Mater. Chem. C* **2017**, *5*, 2074–2083. [[CrossRef](#)]
98. Nazari, M.; Martell, M.; Welsh, T.A.; Melville, O.; Li, Z.; Cann, J.; Cieplechowicz, E.; Zou, Y.; Lessard, B.H.; Welch, G.C. Benzyl and Fluorinated Benzyl Side Chains for Perylene Diimide Non-Fullerene Acceptors. *Mater. Chem. Front.* **2018**, *2*, 2272–2276. [[CrossRef](#)]
99. Dayneko, S.V.; Hendsbee, A.D.; Welch, G.C. Combining Facile Synthetic Methods with Greener Processing for Efficient Polymer-Perylene Diimide Based Organic Solar Cells. *Small Methods* **2018**, *2*, 1800081. [[CrossRef](#)]
100. Laventure, A.; Harding, C.R.; Cieplechowicz, E.; Li, Z.; Wang, J.; Zou, Y.; Welch, G.C. Screening Quinoxaline-Type Donor Polymers for Roll-to-Roll Processing Compatible Organic Photovoltaics. *ACS Appl. Polym. Mater.* **2019**, *1*, 2168–2176. [[CrossRef](#)]
101. Tintori, F.; Laventure, A.; Welch, G.C. Perylene Diimide Based Organic Photovoltaics with Slot-Die Coated Active Layers from Halogen-Free Solvents in Air at Room Temperature. *ACS Appl. Mater. Interfaces* **2019**, *11*, 39010–39017. [[CrossRef](#)] [[PubMed](#)]
102. Abd-Ellah, M.; Cann, J.; Dayneko, S.V.; Laventure, A.; Cieplechowicz, E.; Welch, G.C. Interfacial ZnO Modification Using a Carboxylic Acid Functionalized N-Annulated Perylene Diimide for Inverted Type Organic Photovoltaics. *ACS Appl. Electron. Mater.* **2019**, *1*, 1590–1596. [[CrossRef](#)]
103. Dayneko, S.V.; Hendsbee, A.D.; Cann, J.R.; Cabanetos, C.; Welch, G.C. Ternary Organic Solar Cells: Using Molecular Donor or Acceptor Third Components to Increase Open Circuit Voltage. *New J. Chem.* **2019**, *43*, 10442–10448. [[CrossRef](#)]
104. Farahat, M.E.; Laventure, A.; Anderson, M.A.; Mainville, M.; Tintori, F.; Leclerc, M.; Ratcliff, E.L.; Welch, G.C. Slot-Die-Coated Ternary Organic Photovoltaics for Indoor Light Recycling. *ACS Appl. Mater. Interfaces* **2020**, *12*, 43684–43693. [[CrossRef](#)]
105. Dayneko, S.V.; Pahlevani, M.; Welch, G.C. Indoor Photovoltaics: Photoactive Material Selection, Greener Ink Formulations, and Slot-Die Coated Active Layers. *ACS Appl. Mater. Interfaces* **2019**, *11*, 46017–46025. [[CrossRef](#)] [[PubMed](#)]
106. Payne, A.-J.; Rice, N.A.; McAfee, S.M.; Li, S.; Josse, P.; Cabanetos, C.; Risko, C.; Lessard, B.H.; Welch, G.C. Donor or Acceptor? How Selection of the Rylene Imide End Cap Impacts the Polarity of  $\pi$ -Conjugated Molecules for Organic Electronics. *ACS Appl. Energy Mater.* **2018**, *1*, 4906–4916. [[CrossRef](#)]
107. Welsh, T.A.; Nazari, M.; Welch, G.C. Diketopyrrolopyrrole Derivatives Functionalized with N-Annulated PDI and Se-Annulated PDI by Direct (Hetero)Arylation Methods. *Asian J. Org. Chem.* **2020**, *9*, 1291–1300. [[CrossRef](#)]
108. Sun, K.; Xiao, Z.; Hanssen, E.; Klein, M.F.G.; Dam, H.H.; Pfaff, M.; Gerthsen, D.; Wong, W.W.H.; Jones, D.J. The Role of Solvent Vapor Annealing in Highly Efficient Air-Processed Small Molecule Solar Cells. *J. Mater. Chem. A* **2014**, *2*, 9048–9054. [[CrossRef](#)]
109. Cann, J.R.; Cabanetos, C.; Welch, G.C. Spectroscopic Engineering toward Near-Infrared Absorption of Materials Containing Perylene Diimide. *ChemPlusChem* **2017**, *82*, 1359–1364. [[CrossRef](#)]
110. Barbon, S.M.; Staroverov, V.N.; Gilroy, J.B. Effect of Extended  $\pi$  Conjugation on the Spectroscopic and Electrochemical Properties of Boron Difluoride Formazanate Complexes. *J. Org. Chem.* **2015**, *80*, 5226–5235. [[CrossRef](#)]
111. Ren, Y.; Jäkke, F. Merging Thiophene with Boron: New Building Blocks for Conjugated Materials. *Dalton Trans.* **2016**, *45*, 13996–14007. [[CrossRef](#)] [[PubMed](#)]
112. Romero-Nieto, C.; Baumgartner, T. Dithieno[3,2-b:2',3'-d]Phospholes: A Look Back at the First Decade. *Synlett* **2013**, *24*, 920–937. [[CrossRef](#)]
113. Jo, J.; Pron, A.; Berrouard, P.; Leong, W.L.; Yuen, J.D.; Moon, J.S.; Leclerc, M.; Heeger, A.J. A New Terthiophene-Thienopyrrolodione Copolymer-Based Bulk Heterojunction Solar Cell with High Open-Circuit Voltage. *Adv. Energy Mater.* **2012**, *2*, 1397–1403. [[CrossRef](#)]
114. Zhao, W.; Qian, D.; Zhang, S.; Li, S.; Inganäs, O.; Gao, F.; Hou, J. Fullerene-Free Polymer Solar Cells with over 11% Efficiency and Excellent Thermal Stability. *Adv. Mater.* **2016**, *28*, 4734–4739. [[CrossRef](#)] [[PubMed](#)]
115. You, F.; Zhou, X.; Huang, H.; Liu, Y.; Liu, S.; Shao, J.; Zhao, B.; Qin, T.; Huang, W. N-Annulated Perylene Diimide Derivatives as Non-Fullerene Acceptors for Solution-Processed Solar Cells with an Open-Circuit Voltage of up to 1.14 V. *New J. Chem.* **2018**, *42*, 15079–15087. [[CrossRef](#)]
116. Li, C.; Fu, H.; Xia, T.; Sun, Y. Asymmetric Nonfullerene Small Molecule Acceptors for Organic Solar Cells. *Adv. Energy Mater.* **2019**, *9*, 1900999. [[CrossRef](#)]
117. Yin, Y.; Song, J.; Guo, F.; Sun, Y.; Zhao, L.; Zhang, Y. Asymmetrical vs Symmetrical Selenophene-Annulated Fused Perylenediimide Acceptors for Efficient Non-Fullerene Polymer Solar Cells. *ACS Appl. Energy Mater.* **2018**, *1*, 6577–6585. [[CrossRef](#)]
118. Koenig, J.D.B.; Hoff, A.; Gasonoo, A.; Welch, G.C. Systematic Investigation of Core and Endcap Selection on the Development of Functional  $\pi$ -Conjugated Materials. *Chem. Mater.* **2023**, *35*, 251–260. [[CrossRef](#)]
119. Hoff, A.; Martell, M.; Gasonoo, A.; Koenig, J.D.B.; Simón Marqués, P.; Cieplechowicz, E.; Pahlevani, M.; Welch, G.C. Sidechain-Engineered N-PDIs Processed from Ethyl Acetate as Effective Cathode Interlayers for Organic Solar Cells. *Adv. Eng. Mater.* **2022**, 2201437. [[CrossRef](#)]
120. Hoff, A.; Gasonoo, A.; Pahlevani, M.; Welch, G.C. An Alcohol-Soluble N-Annulated Perylene Diimide Cathode Interlayer for Air-Processed, Slot-Die Coated Organic Photovoltaic Devices and Large-Area Modules. *Sol. RRL* **2022**, *6*, 2200691. [[CrossRef](#)]

121. Farahat, M.E.; Anderson, M.A.; Martell, M.; Ratcliff, E.L.; Welch, G.C. New Perylene Diimide Ink for Interlayer Formation in Air-Processed Conventional Organic Photovoltaic Devices. *ACS Appl. Mater. Interfaces* **2022**, *14*, 43558–43567. [[CrossRef](#)] [[PubMed](#)]
122. Munir, R.; Cieplechowicz, E.; Lamarche, R.M.; Chernikov, R.; Trudel, S.; Welch, G.C. Air-Processed Organic Photovoltaics for Outdoor and Indoor Use Based upon a Tin Oxide-Perylene Diimide Electron Transporting Bilayer. *Adv. Mater. Interfaces* **2022**, *9*, 2101918. [[CrossRef](#)]
123. Cieplechowicz, E.; Munir, R.; Anderson, M.A.; Ratcliff, E.L.; Welch, G.C. Zinc Oxide-Perylene Diimide Hybrid Electron Transport Layers for Air-Processed Inverted Organic Photovoltaic Devices. *ACS Appl. Mater. Interfaces* **2021**, *13*, 49096–49103. [[CrossRef](#)] [[PubMed](#)]

**Disclaimer/Publisher's Note:** The statements, opinions and data contained in all publications are solely those of the individual author(s) and contributor(s) and not of MDPI and/or the editor(s). MDPI and/or the editor(s) disclaim responsibility for any injury to people or property resulting from any ideas, methods, instructions or products referred to in the content.